J Physiol 592.16 (2014) pp 3625–3646

The Journal of Physiology

Spatial effects of shifting prisms on properties of posterior parietal cortex neurons

Anushree N. Karkhanis, Barbara Heider, Fabian Muñoz Silva and Ralph M. Siegel

Center for Molecular and Behavioral Neuroscience, Rutgers University, Newark, NJ, USA

Key points

- The posterior parietal cortex contains multiple spatial representations and is involved in online monitoring of visually guided hand movements.
- Single unit recordings were performed in two areas of macaque monkey posterior parietal cortex during a visually guided reaching task with variable eye position.
- To test the adaptability of neural responses, shifting prisms were introduced to create a discrepancy between perceived and actual reach location.
- The majority of neurons changed average firing rate and/or eye position tuning during the prism exposure.
- The direction of tuning change did not correlate with the direction of prism shift, suggesting more generalized network effects due to the perturbation.
- Population analysis using Euler angles and translations demonstrated systematic transformations between conditions supporting the notion of network behaviour.

Abstract The posterior parietal cortex contains neurons that respond to visual stimulation and motor behaviour. The objective of the current study was to test short-term adaptation in neurons in macaque area 7a and the dorsal prelunate during visually guided reaching using Fresnel prisms that displaced the visual field. The visual perturbation shifted the eye position and created a mismatch between perceived and actual reach location. Two non-human primates were trained to reach to visual targets before, during and after prism exposure while fixating the reach target in different locations. They were required to reach to the physical location of the reach target and not the perceived, displaced location. While behavioural adaptation to the prisms occurred within a few trials, the majority of neurons responded to the distortion either with substantial changes in spatial eye position tuning or changes in overall firing rate. These changes persisted even after prism removal. The spatial changes were not correlated with the direction of induced prism shift. The transformation of gain fields between conditions was estimated by calculating the translation and rotation in Euler angles. Rotations and translations of the horizontal and vertical spatial components occurred in a systematic manner for the population of neurons suggesting that the posterior parietal cortex retains a constant representation of the visual field remapping between experimental conditions.

(Received 6 February 2014; accepted after revision 5 June 2014; first published online 13 June 2014)
Corresponding author B. Heider: Center for Molecular and Behavioral Neuroscience, Rutgers, The State University of New Jersey, 197 University Avenue, Newark, NJ 07102, USA. Email: heibarbara@gmail.com

Abbreviations C, main condition effect; C×P, interaction effect condition × position; DP, dorsal prelunate area; IPS, intraparietal sulcus; LS, lunate sulcus; MVT, movement time; NS, non-significant; PMd, dorsal premotor area; PPC, posterior parietal cortex; PRR, parietal reach region; RT, reaction time; STS, superior temporal sulcus.

Ralph M. Siegel passed away 2 September 2011.

DOI: 10.1113/jphysiol.2014.270942

Introduction

Neurons in the posterior parietal cortex (PPC) of the macaque monkey are involved in sensorimotor transformation essential for visually guided behaviours (Mountcastle *et al.* 1975; MacKay, 1992; Battaglia-Mayer *et al.* 2005; Heider *et al.* 2010*a*). Visual responses of neurons in multiple parietal areas are strongly modulated by eye position, often referred to as *gain fields* (Andersen *et al.* 1985, 1990; Li *et al.* 1989; Galletti *et al.* 1995; Read & Siegel, 1997). Other sources of modulation such as attention (Mountcastle *et al.* 1981; Steinmetz *et al.* 1994; Quraishi *et al.* 2007; Galletti *et al.* 2010) or visually directed hand movements (Fattori *et al.* 2005; Battaglia-Mayer *et al.* 2007; Heider *et al.* 2010*a*; Hadjidimitrakis *et al.* 2013) have been confirmed. Thus, spatial gain field tuning can be altered depending on the task requirements.

Various representations converge in the parietal cortex, which is considered crucial for dynamic updating of actions. Testing neural responses during visual perturbation might shed further light on how these signals converge in PPC. Direct electrophysiological evidence for adaptive changes in response to different types of perturbation has been provided for neurons in the motor and premotor cortex (Kurata & Hoshi, 2002; Padoa-Schioppa *et al.* 2004). As the PPC neurons are involved in the online correction process during visually guided reaching (Bosco *et al.* 2010), the mismatch between perceptual and physical reach target will probably affect gain field tuning in PPC neurons. To test this hypothesis, two macaque monkeys performed a visually guided reaching task, during which Fresnel prisms displaced the foveated reach targets. Two areas of the PPC were studied, area 7a and the dorsal prelunate (DP). Our results show that the gain field tuning and overall firing rate of the majority of area 7a and DP neurons changed substantially with the prism distortion, and that in most neurons these changes persisted after removal of the prism.

Methods

Ethical approval

Two male rhesus monkeys (*Macaca mulatta*, M1R 11 kg, M3R 8.5 kg; both between 10 and 12 years of age) were trained on a visually guided reaching (VGR) task as described below. All experimental and surgical procedures were in accordance with the National Institute of Health *Guide for the Care and Use of Laboratory Animals* and approved by the Rutgers University Institutional Animal Care and Use Committee (IACUC).

Animal preparation

At the time of the reaching studies, both monkeys had already been extensively trained in various visual tasks during which they had to release a lever upon detecting a stimulus change. Both monkeys had been implanted with a head post and cranial chambers for optical imaging studies about 7 years previously (Siegel *et al.* 2003; Heider *et al.* 2005). All surgical procedures were performed under sterile conditions and veterinary supervision. Anaesthesia was initiated with ketamine (10 mg kg^{-1} I.M.) and atropine (0.04 mg kg^{-1} I.M. or S.C.) and maintained by inhalation isoflurane (0.5–4%) in oxygen (5 l min^{-1}). Antibiotics (ceftriaxone 50 mg kg^{-1} I.V. or I.M.) were administered prophylactically during surgery and postoperatively for at least 1 week. Postoperative analgesics were given at least twice per day (buprenorphine 2–6 μg kg^{-1} I.M.). In both animals, a stainless steel head post was implanted first after the initial training period without head restraint. The head post was embedded in bone cement (Palacos®, Heraeus Medical, Wehrheim, Germany) anchored to the skull with 15–20 craniofacial titanium screws (Synthes, West Chester, PA, USA). After recovery from surgery (10–14 days), training of the visual task continued by gradually familiarizing the monkeys with the head restraint and eye movement monitoring. This training period typically lasted 2–3 months until the monkeys achieved an adequate performance level [i.e. reaction times (RT), precision of fixation]. In the second surgery, a stainless steel optical chamber (20 mm outside diameter) was implanted over the right hemisphere in each animal. The skull was removed within the chamber using a manual trephine; the dura was resected and replaced with a transparent artificial dura according to published methods (Shtoyerman *et al.* 2000; Arieli *et al.* 2002).

After conclusion of the optical imaging studies, the artificial dura was removed under ketamine sedation (5–10 mg kg^{-1} I.M.), and the natural dura regrew within a few days. A stainless steel adapter was attached to the optical chamber in order to secure the stage and the microdrive. This set-up permitted precise electrode penetrations in both monkeys (Fig. 1*A*). Recordings were conducted in the right hemisphere of both animals. Both animals performed the VGR task using their left contralateral hand. This task differed from a 'classical gain field' task where fixation was combined with a lever release (Andersen & Mountcastle, 1983; Andersen *et al.* 1987; Read & Siegel, 1997). The reaching studies were performed over 3 years. Owing to limitations in the experimental set-up, one monkey was studied at a time for a period of 2–6 months while the other monkey rested. This resulted in a total recording time of 8–12 months per monkey. As one experiment could last up to 5 h, two to three experimental sessions were performed per week. After conclusion of the reaching studies, both monkeys continued participating in other electrophysiological and imaging studies (Heider *et al.* 2010*b*; Heider & Siegel, 2014) until they were killed with an overdose of pentobarbital (50 mg kg^{-1} I.V.).

Experimental set-up

The monkeys were seated in a custom-built primate chair, which allowed them to freely move their upper limbs. Their heads were immobilized using the implanted head holder. A touch screen monitor (diameter 45 cm; Elo TouchSystems, Menlo Park, CA, USA) recorded the reaching end-points and was positioned 29 cm or 35 cm (depending on each monkey's arm length) away from the eyes. A capacitive proximity sensor (KD5041; IFM Electronic Inc., Exton, PA, USA) was placed on the primate chair close to the torso at the waist level. This sensor provided a touch sensitive surface area of 25 cm^2 and positioned the hand at a constant starting position for every trial. Distance from the hand's starting position to the touch screen was between 34 cm and 40 cm depending on the target position. The display size and monitor distance was designed so that each monkey was able to reach all nine targets comfortably. A clear prism holder was mounted in front of the monkey's face; it did not obstruct the view of the touch screen and the Fresnel prism could easily be attached to the holder. An infrared eye-tracking camera (RK-416; ISCAN, Cambridge, MA, USA) monitored the eye position at 60 Hz throughout the trial and ensured that fixation was maintained within 4° in accordance with previous reaching studies (Batista & Andersen, 2001; Battaglia-Mayer *et al.* 2005; Snyder *et al.* 2006). The stimulus display and collection of behavioural measures from the eye camera and touch screen were programmed using the NIMH Cortex software (http://dally.nimh.nih.gov), which was also synchronized with the analog spike collection system. The experiments were performed in darkness; however, some luminance from the touch screen monitor was observed at the lowest brightness and black background settings.

Behavioural task

The fixation point was a small red square (diagonal 4 mm, ∼0.8°). The visual stimuli used as reach targets were circular expanding optic flow patches (diameter 7.5 cm, 12°–14°; consisting of 128 dots, diameter 1 mm, ∼0.2°). The dots moved in an outward direction with the fixation point as the reference point (velocity of 6° s^{-1}, point life of 532 ms). The optic flow stimulus was chosen, as neurons in areas 7a and DP respond well to these stimuli (Tanaka *et al.* 1986; Siegel & Read, 1997; Merchant *et al.* 2001).

Both monkeys were trained to perform the VGR task with and without prism. The task was identical to the 'eye position-varied reaching task' described in a previous study (Heider *et al.* 2010*a*). Each trial lasted for a maximum of 8000 ms (Fig. 1*B*) and began with the monkey's hand resting on the touch sensor placed on the primate chair close to the trunk. Once the hand activated the touch sensor, the red fixation point appeared on the touch screen in one of nine positions. Constant fixation was required throughout the trial. After 1500 ms, the reach target appeared centred behind the fixation point. Between 2000 and 3000 ms after stimulus onset, the expanding motion of the optic flow became unstructured; this cued the monkey to reach to the visual stimulus. Thus, the eye position and the reach position were always congruent resulting in a 'foveal' reach. The monkeys were required to move their hand as fast as possible with little visual feedback. These are the requirements for a ballistic reach, which is characterized by a single peaked velocity profile without corrective movements (Vercher *et al.* 1994; Desmurget *et al.* 2005; Caselli *et al.* 2006). The darkened room and the placement of the starting position of the hand close to the torso minimized the visual feedback. Consequently, the monkey's hand entered their visual field only when it was close to the reach end-point. We cannot exclude the visual effect of the hand approaching the optic flow target. However, as the target itself already consisted of 128 randomly moving dots, an additional moving stimulus consisting mostly of the monkey's finger coming in the field of view was unlikely to substantially alter the neural response.

The RT to lift the hand off of the sensor plus the movement time (MVT) to reach the screen could not exceed 1000 ms or the trial was aborted. After a correct touch of the stimulus, the monkey was required to hold the hand on the screen for 1500 ms. A juice reward and the offset of the visual stimulus marked the end of a successful trial. The different target locations within a sub-block were presented in pseudo-randomized order.

If at any time during the trial the fixation was interrupted, the hand was launched outside the given time, or an erroneous reach was made (either by reaching outside the visual stimulus radius or by not holding the hand to the visual stimulus for sufficient time), the trial was aborted immediately. A new trial was initiated once the hand was again on the proximity sensor. The missed location was repeated in a pseudo-randomized order within each sub-block, which consisted of nine correct trials (one for each location). The monkeys were required to complete all nine reaches correctly in each sub-block to proceed to the next sub-block. A block consisted of 10 such sub-blocks resulting in 90 correct trials.

To investigate the effects of perceptual distortion, the VGR task was performed under three different conditions. In the *pre-prism* condition (first block), monkeys performed the VGR task with the prism holder in place but without the prism inserted. In the *prism* condition (second block), a 12° Fresnel prism (Fresnel Prism & Lens Co., LLC, Eden Prairie, MN, USA), which shifted the visual field by 12°, was inserted into the holder. The exact prismatic distortion was measured with a laser beam for all nine target positions and was confirmed to be uniform. The prismatic distortion was applied in

one of four cardinal directions: upward (90°), downward (270°), contralateral (180°) or ipsilateral (0°). In those cases where the initial eye position tuning could be established qualitatively during the pre-prism condition, the prism shift was chosen along the same axis as the gain field either in the opposite or in the same direction. In most experiments, however, the eye position tuning could not be established unequivocally during the recording, thus the direction of the prism shift was chosen randomly. In addition, certain shifts proved to be more difficult, the monkeys were reluctant to perform and a different direction had to be used. This resulted in an unequal number of experiments for each of the four possible shifts. Each neuron was tested for only one shift direction.

With the prism the entire display was perceptually displaced, which created a mismatch between the perceived and actual target position. The perceptual shift was accompanied by a small shift in eye position (Fig. 2*C*). The monkeys were required to reach to the actual location of the target. If the monkeys reached outside the target it was considered an incorrect reach and the trial was aborted. The initial reaches during prism conditions often landed at the edge of the optic flow target. The highly trained monkeys corrected their reaches to attain the actual target location within a few trials. Finally, for the *post-prism* condition (third block) the prism was removed and the monkeys repeated the VGR task to test the behavioural and neural recovery. Analogous to the prism condition, the monkeys adapted quickly to the absence of the prism. The completion of the post-prism condition was dependent on the stability of the recording and the performance and motivation of the monkeys. Thus, some recordings consisted only of the pre-prism and prism conditions or in some cases an incomplete post-prism condition. Each block was completed in approximately 40 min depending on the monkeys' performance. The completion of the entire set of three blocks required about 2 h. To confirm that the neural effects observed were truly due to the perceptual distortion and not artefactual (e.g. neural instability or fluctuations), monkey M3R performed two consecutive blocks of the VGR task with only the clear glass prism holder in place (*control1* and *control2*). These paired control recordings were interspersed with the prism experiments.

Neural recordings

Extracellular single unit recordings were conducted by electrical measurements from DC to 20 kHz using platinum-iridium, glass-coated microelectrodes (UEPSEGSG2N5G; FHC, Bowdoinham, ME, USA) with an impedance of 0.5–2.5 MΩ. The electrode was advanced through the dura using a hydraulic microdrive (Model 650; David Kopf Instruments, Tujunga, CA, USA) attached to the recording chamber via a stainless steel adapter. The coordinate system on the microdrive combined with the previous optical images of the brain allowed targeted recordings. Areas 7a and DP of the PPC were identified using the vascular pattern over the gyri bounded by the lunate, intraparietal and superior temporal sulci visible under the transparent artificial dura (Fig. 1*A*).

The electrode was inserted approximately orthogonal to the dural surface. The depth of the recording was quantified during advancing and retracting based on the first and last occurrence of neural signals. The neural signal was amplified (Model 1800 Microelectrode AC Amplifier; A-M Systems, Carlsborg, WA, USA), and then filtered using a 50/60 Hz noise eliminator Humbug (Auto-Mate Scientific, Berkley, CA, USA) and a band-pass filter (300 Hz–20 kHz). A Matlab (MathWorks, Natick, MA, USA) based analog signal collection system along with a PCMCIA-based analog-to-digital converter (NIDAQ Card-6036E; National Instruments, Austin, TX, USA) was used to collect the data. The neural activity was digitized at 40 kHz. Activity from every neuron that was sufficiently isolated was recorded regardless of the neuron's eye position tuning or preference for any aspect of the VGR task. Online isolation of neurons was done using a dual-window discriminator (DIS-I; BAK Electronics, Germantown, MD, USA) to qualitatively assess neural selectivity and spatial preference during recording.

Spike analysis

Single unit responses were recorded during all phases of the task to assess temporal and spatial aspects of neural modulation. For the off-line analysis, analog data were sorted using the Plexon software (Plexon Offline Sorter 1.39; Plexon, Dallas, TX, USA). All subsequent quantitative analyses were performed on these offline-sorted data. Spike rasters were synchronized to different events during each trial and the firing rate was calculated for four epochs of interest (Fig. 1*C*). (1) The *fixation epoch* was defined as the time interval of 500 ms before the onset of the visual stimulus. Only the red fixation point was displayed in one of nine positions and the monkey maintained fixation. As the visual effect of the fixation point was minimal, neural spatial modulation during this epoch was largely due to eye position signals. (2) The *visual epoch* was defined as the 500 ms time interval after the onset of the visual stimulus. The gain field tuning was defined as the eye position-dependent visual response (Andersen *et al.* 1985, 1990; Read & Siegel, 1997; Siegel *et al.* 2003). (3) The *preparatory epoch* was defined as the 500 ms time interval immediately before the stimulus changed from structured to unstructured motion to avoid contamination by overt changes in stimulus or motor behaviours. The visual stimulus was constant during this

time interval and the hand was still steady on the starting position (between 2000 and 3000 ms after stimulus onset). Changes in neural activity during this epoch are thus probably due to internal processing (i.e. reach preparation or planning). (4) The *reach epoch* was defined as the 300 ms time interval following the lift hand event. The shorter time interval was chosen to avoid the sensory stimulation caused by the hand moving into the visual field during the latter part of the reach movement and the tactile stimulation from contact with the monitor. We considered using an even shorter epoch (200 or 250 ms) and found that the results of the regression were unchanged, thus decided to stay with the 300 ms analysis epoch. This also allowed us to keep the data comparable to our reaching study without prisms where we utilized a 300 ms epoch (Heider *et al.* 2010*a*).

Statistical analysis

Temporal spike analysis. The interspike interval (ISI) return maps summarize the temporal dynamics of single unit spiking activity and therefore can confirm the identity of a neuron throughout a prolonged recording period. Plotting the points ISI(i+1) against ISI(i), where ISI(i) is the ith ISI, creates these neural 'fingerprints'. ISI return maps were created for all correct trials for each pairing of conditions (pre-prism *vs.* prism, pre-prism *vs.* post-prism), as demonstrated for a previous study (Quraishi *et al.* 2007). Logarithmic axes (base 10) were applied to visualize the wide dynamic range from 0.1 ms to 10,000 ms. The similarity of the paired ISI return maps were compared by converting each of the return maps to two-dimensional density plots $\Psi(I,J)/N$, where N is the number of spikes. The root mean square error (Ξ) between the paired density plots was used as a similarity measure: A small Ξ indicated that the two ISI return maps were similar, which strongly suggests that the same temporal pattern, and by extension, the same neuron was recorded under both conditions. A large Ξ suggests that the neuron changed its firing pattern, which is indicative of a loss of recording stability or a change in firing rate. The Ξ between all possible pairs was computed. For example, a pre-prism run for a particular cell was compared to all prism and pre-prism runs of every cell. The resulting set of Ξ values was split into those from actual pairings and those synthetically generated by all the other pairings. The marginal probability was computed for all the actual pairings by determining the fraction of measurements with Ξ values less than a particular neuron. Based on the ISI maps, neurons with insufficient stability were excluded from further analyses. The findings from the ISI analysis were confirmed by examining the waveforms for each neuron across conditions using the Matlab-based package *Wave_clus* (Quiroga *et al.* 2004).

Categorical regression analysis. A multistep method was used to quantify and directly compare the spatial tuning across conditions. First, the firing rate for each of the four epochs, fixation, visual, preparatory and reach epoch, was computed. Second, categorical regression analysis was used to compute the spatial and the intercept parameters, which were then used to classify the units by type of interaction. Third, regressions with categorical variables denoting the different conditions explained below quantified changes in the spatial tuning. A stepwise categorical linear model was used to simultaneously examine the dependency of firing rate on the condition for each epoch (condition-based comparison):

$$A(x, y, C, i) = (a_x + a_{xc})x + (a_y + a_{yc})y + (a + a_c)C + \varepsilon_i \quad (1)$$

where $A(x,y,C,i)$ corresponds to the firing rate at the ith trial. The term c denotes conditions and therefore has two categorical values (pre-prism–prism, pre-prism–post-prism). The variables x and y correspond to the horizontal and vertical location of the stimulus, respectively. The term a_x corresponds to the linear deviation for the horizontal component. Therefore, the term $(a_x + a_{xc})x$ corresponds to the coefficient for the linear dependence on the horizontal position of the stimulus for one of the two categories. The term a_y is the linear deviation coefficient for the vertical component. The term $(a_y + a_{yc})y$ corresponds to the coefficient for the linear dependence on the vertical position of the stimulus. The intercept term $(a + a_c)C$ is the modelled firing rate of the neuron for the foveal stimulus at 0°, 0° and the term ε_i is the residual error. Each parameter was considered but only the significant ($P < 0.05$) parameters remained in the final equation. The categorical regression was implemented using GLMOD and REG procedures (SAS Institute Inc., Cary, NC, USA). To assess the initial gain field tuning of each neuron before any perturbation, a linear regression analysis (without quadratic components) was applied for the visual epoch according to previous studies (Andersen *et al.* 1985; Bremmer *et al.* 1997; Read & Siegel, 1997). The categorical regression for the pre-prism *vs.* prism comparison quantified the changes before and during the perceptual perturbation. The pre-prism *vs.* post-prism comparison tested whether the neurons regained the tuning properties after the distortion was removed. A three-level comparison was not useful because it simply determined if spatial tuning altered for one of the three conditions, without specifying exactly which one was different. For this reason and due to the fact that the third condition (post-prism) was not available for all neurons, the categorical regression was performed between the paired conditions.

The spatial tuning for each epoch (fixation, visual, preparatory and reach) during pre-prism condition

was compared to the respective epoch in the prism condition. Neurons were classified into one of three classes: (1) neurons that were not spatially tuned but changed their overall firing rate between conditions (type C); (2) neurons with significant changes in spatial tuning across conditions had a multiplicative interaction between condition and the position (type C×P; some but not all of these cells also changed their overall firing rate, intercept term); (3) neurons without eye position tuning and constant overall firing rate across conditions (non-significant, NS). Two other types that could result from the categorical regression analysis were not encountered (Heider *et al.* 2010*a*). The distribution of tuning types between areas was analysed with a chi-squared test (significance level $P < 0.05$). The direction of spatial tuning for each neuron was derived from the linear horizontal and vertical coefficients, which defined the vectors that were then transformed into polar coordinates: $\theta =$ arc tan (a_y/a_x) with the convention 0° (360°) corresponding to the ipsilateral eye position along the horizontal meridian.

The spatial distribution of the population vectors was analysed using circular statistics (Batschelet, 1981; Zar, 1984). The Hotelling test determined if the resulting population vectors had a significant mean direction. Significant F values ($P < 0.05$) indicate a non-uniform distribution of angles. To determine the shifts in spatial tuning between the two conditions, the difference vectors were computed for the prism–pre-prism ($a_{x(\text{prism})} - a_{x(\text{pre-prism})}$ and $a_{y(\text{prism})} - a_{y(\text{pre-prism})}$) and post-prism–pre-prism ($a_{x(\text{post-prism})} - a_{x(\text{pre-prism})}$ and $a_{y(\text{post-prism})} - a_{y(\text{pre-prism})}$) comparisons. The difference vector length thus designates the magnitude of the tuning change. Similarly, for neurons with significant intercept terms (all type C and some of type C×P), the intercept difference between conditions indicates the magnitude of change in average firing rate.

Transformation analysis. The gain field tuning of each neuron can be modelled as a plane in 3D space using the parameters from the linear regression. (Quraishi *et al.* 2007; Heider *et al.* 2010*a*). Thus, two planes per epoch illustrate the change in spatial tuning and firing rate. To generalize the spatial changes for the two gain fields between conditions, we applied a transformation analysis commonly used in kinematics. We defined the state of the neuron as a position in 3D space with the linear combination of spatial domain (x and y as horizontal and vertical target position, respectively) and the intercept as z (height of the modelled plane). We generated 72 positions to represent the complete visual angular surface of 36°× 36° and its respective firing rate derived from the linear regression. To relate the two neural states (pre-prism–prism, pre-prism–post-prism), we propose a transformation between the two conditions (planes). In general, for any pair of planes, U and V, it is possible to find a decomposition of rotations and translation with respect to reference using the following equation:

$$T(U) = RU + t = V$$

With R being the rotation matrix (3 × 3) and t the translation matrix (3 × 1). The rotation matrix (R) was resolved with the following steps. The first step was a singular value decomposition on to a covariance matrix $S = UV^{\mathrm{T}}$ with U being the pre-prism vectors and V being the prism vectors: $S = X\Sigma Y^{\mathrm{T}}$. X and Y are unitary column vectors, each of which forms a set of orthonormal vectors. The second step was the evaluation of the rotation matrix as follows: $R = X^{\mathrm{T}}\ Y$. The accuracy between RU and V was checked with the root mean square and the difference for all cases was less than 10^{-6}. Finally, the translation matrix t was determined using $t = <V> - R <U>$ with $< >$ representing the mean of the components of the set to generate the centroid. Both rotation and translation revealed the remapping of spatial tuning for each neuron affected by the prism. This approach calculated the transformation between pre-prism and prism as well as between pre-prism and post-prism separately for each epoch. The rotation matrix (R) can be expressed in terms of Euler angles as $R = R_z(\gamma)\ R_y(\beta)\ R_x(\alpha)$ (Waldron & Schmiedeler, 2008).

$$Rx(\alpha) = \begin{pmatrix} 1 & 0 & 0 \\ 0 & \cos\alpha & \sin\alpha \\ 0 & -\sin\alpha & \cos\alpha \end{pmatrix}$$

$$Ry(\beta) = \begin{pmatrix} \cos\beta & \sin\beta & 1 \\ -\sin\beta & \cos\beta & 0 \\ 0 & 0 & 0 \end{pmatrix}$$

$$Rz(\gamma) = \begin{pmatrix} 1 & 0 & 0 \\ 0 & \cos\gamma & \sin\gamma \\ 0 & -\sin\gamma & \cos\gamma \end{pmatrix}$$

These Euler angles are a set of three angles (α, β, γ) specifying the change of orientation in space of a rigid body, which in our case correspond to the gain fields of a neuron in PPC. The body's position is altered by a rotation of body axes through an angle α along the body's x-axis, β along the y-axis and γ along the z-axis. For the current study, the analysis focused on the α and β angles representing the changes of the two spatial parameters. The distributions of these angles were fit with a regular sinusoidal function. Similarly, the translation will focus on the changes in x and y. The distribution of the translation values was fit with a linear regression, whereby the outliers were assigned a smaller weight (*robustfit*; Matlab Statistics Toolbox™; MathWorks) to allow a more 'truthful' fit. Only fits with an $R^2 \geq 0.5$ were considered. An equivalent representation to Euler

angles, supported by Euler's rotation theorem, is to derive a unitary vector ($\hat{\mathbf{e}}$) and an angle (θ) of revolution about that vector that describes the magnitude of the rotation in the sense prescribed by the right-hand rule about the axis (Waldron & Schmiedeler, 2008). This is referred to as angle-axis representation. Here r_{ij} corresponds to the components of the rotation matrix as computed previously.

$$\theta = \cos^{-1}\left(\frac{r_{11} + r_{22} - r_{33} - 1}{2}\right)$$

$$\hat{\mathbf{e}} = \frac{1}{2\sin\theta}\begin{pmatrix} r_{32} - r_{23} \\ r_{13} - r_{31} \\ r_{21} - r_{12} \end{pmatrix}$$

Results

Behavioural effects of perceptual perturbation

The highly trained monkeys reached accurately to all targets during the pre-prism condition, although both showed some systematic bias during the first block (see Heider *et al.* 2010*a*, Fig. 4*A*). This was mainly due to the varying kinematics required for targets at the different heights (Christel & Billard, 2002). During the prism condition they initially 'misreached' to the shifted target locations. With extensive training, the monkeys quickly adapted and reached to the actual location within five to nine trials. After removal of the prism during the post-prism condition, the initial reach end-point was misplaced in the opposite direction relative to the prism shift. This overshoot was also corrected within a few trials.

The average reach errors during the pre-prism, prism and post-prism conditions were computed as the distance between the reach end-point and the centre of the visual stimulus (fixation dot). Reach end-points from one experiment are plotted for all three conditions (Fig. 2*A*). Reaching was most accurate during the pre-prism condition. The initial end-points during the prism condition (12° downward) were shifted in the direction of the distortion but the monkey reached accurately within a few trials for most locations. Once the prism was removed, the reach precision was restored quickly. Because the monkeys adapted rapidly to the presence and subsequent removal of the prism, the reach errors during prism and post-prism conditions did not differ significantly from the pre-prism condition when averaged across all trials. The amplitude of the initial reach errors was smaller than the optical shift, that is, approximately one-quarter to one-half of the angle of distortion (Fig. 2*B*). These findings are in agreement with human (Cressman & Henriques, 2009) and non-human primate (Kurata & Hoshi, 2002) studies. During prism exposure the eye position was maintained within a 4° radius. The average vertical (Fig. 2*C*) and horizontal (Fig. 2*D*) eye positions were plotted for all three conditions and target positions. Although the vertical eye positions were slightly shifted downward in the blocks in the examples, these differences were not significant when averaged across trials, and confirm that the eye position was largely maintained during the different conditions.

RT and MVT were compared between the pre-prism and prism conditions for 108 recording sessions. RT was computed by subtracting the time of the stimulus change from the time the monkey lifted his hand off the sensor. The RT was significantly greater during the prism condition for 29 of 64 (45%) experiments of M3R (filled black circles; Fig. 3*A*) and for eight of 44 (18%) experiments of M1R (filled grey circles; Fig. 3*A*) as confirmed by a Student's t test. Averaged across all experiments, RTs were significantly longer for the prism condition (Student's $t = -3.86$, $P = 0.0002$). In addition, variability was significantly higher during the prism condition ($F = 0.46$, $P = 0.0002$).

The MVT was computed by subtracting the time at which the monkey lifted his hand off the sensor from the time his hand contacted the touch screen. The MVTs were significantly different for 16 of 64 (25%) experiments of M3R and for 25 of 44 (57%) experiments of M1R (Fig. 3*B*). Across all experiments, MVTs were significantly longer for the prism condition (Student's $t = -2.27$, $P = 0.025$), while variances were similar between conditions. The results from both measures, RTs and MVTs, suggest that the prism distortion indeed affected temporal aspects of behaviour. However, these effects varied considerably between experiments and monkeys.

Neural effects of prismatic distortion

Stability of recordings. Two sets of pairs were compared to confirm the stability during the prolonged recordings: pre-prism *vs.* prism (165 pairs) and pre-prism *vs.* post-prism (105 pairs). The distributions of the Ξ values for each group were significantly different between the actual *vs.* the synthetic group as confirmed by the Kolmogorov–Smirnov goodness-of-fit test ($P < 0.001$). The marginal probability was computed for all the actual pairings by determining the fraction of measurements with Ξ values less than a particular neuron. The distribution of these probabilities for two sets of comparisons demonstrates that 28% and 21% of the cells had marginal probabilities <0.05. The remaining 118 of 165 and 81 of 105 neurons had probabilities ≥ 0.05. The large majority of these values can be explained by differences in firing rate between conditions. About half (53% and 49%) of these neurons had changes in firing

rate >50%, as compared to the neurons with marginal probabilities <0.05, of which only about 10% (9% and 14%) had changes in firing rates >50%. These results indicate that the different blocks (pre-prism, prism and post-prism) were probably recorded from stable single neurons with the same temporal pattern but different firing rates throughout the long experimental sessions (Quraishi *et al.* 2007). Based on the ISI analysis, a total of 13 neurons were excluded from the population. Although the firing rate was substantially higher during the prism condition, the identity of the ISI maps during the pre-prism, prism and post-prism conditions

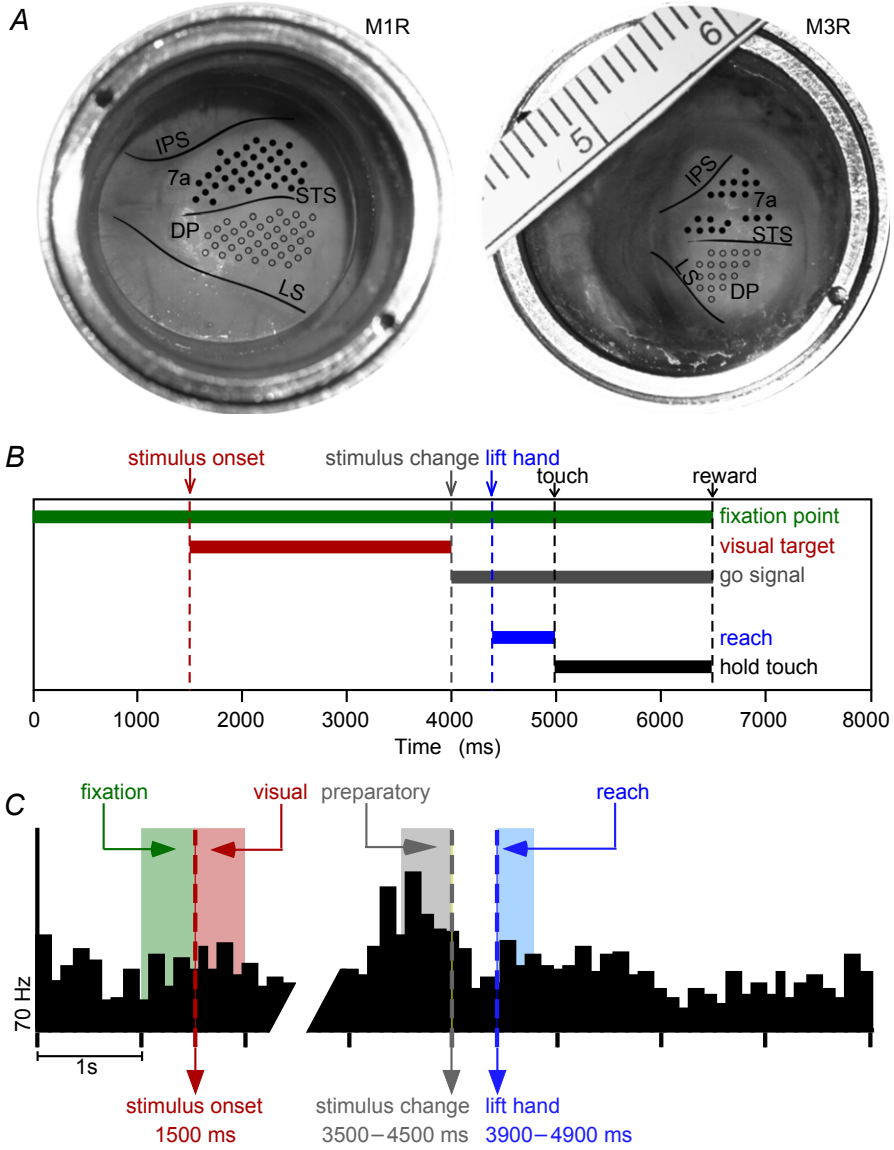

Figure 1. Recording sites, sequence of task events and neural synchronization
A, view through optical chambers (M1R, left; M3R, right; both situated over the right hemisphere). Solid black lines mark sulci visible through the transparent artificial dura; added scale in millimetres. Electrode penetrations in area 7a (filled circles) and the DP (open circles). *B*, sequence of reaching task. Horizontal bars indicate onset and duration of various events within a trial: fixation point, visual target (structured optic flow stimulus), stimulus change (unstructured stimulus), lift hand, touch and hold. Vertical dashed lines mark time points of trial events. *C*, neural synchronization to three trial events with example of a peri-stimulus time histogram (averaged across 10 trials). Time in milliseconds along the horizontal axis, firing rate in Hertz along the vertical axis. Stimulus onset (1500 ms, left dashed line), shaded region to the left indicates fixation epoch and shaded region to the right visual epoch (each 500 ms time intervals). The reach cue (change from structured to unstructured motion) occurred at variable times 2000–3000 ms after stimulus onset. The preparatory epoch consisted of the 500 ms before the cue. The reach epoch consisted of the 300 ms time interval after the hand was lifted off the launch panel. DP, dorsal prelunate; IPS, intraparietal sulcus; LS, lunate sulcus; STS, superior temporal sulcus.

was maintained. The average waveforms confirmed the recording stability.

Single unit activity during pre-prism, prism and post-prism condition. The basic linear regression model, as used previously (Read & Siegel, 1997), established the initial spatial properties before prism application and allowed comparison with previous studies, which were confined to area 7a. Based on this analysis, 46% of area 7a and 28% of area DP neurons had at least one

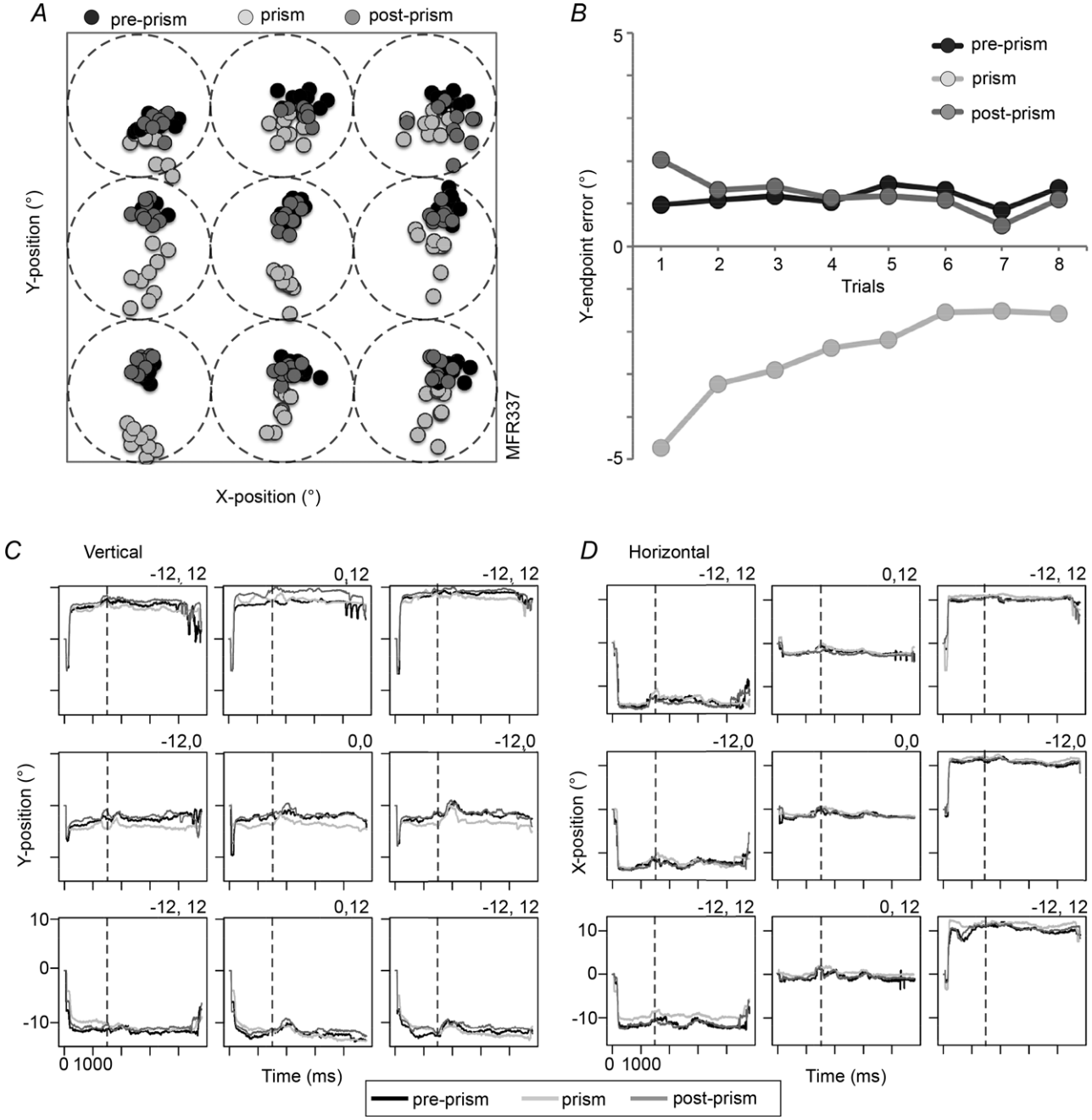

Figure 2. Behavioural parameters during prism adaptation
A, reach end-points for the pre-prism condition (black circles), prism condition (light grey circles) and post-prism condition (medium grey circles) plotted for all nine targets of a typical experiment (M3R337, eight trials per condition). The square illustrates the 36° × 36° touch area. Each dotted circle represents the extent of the optic flow stimulus (diameter 12°) in each of the nine target positions. *B*, vertical end-point errors averaged for all target positions as a function of trial progression. Average vertical (*C*) and horizontal (*D*) eye positions for pre-prism (black lines), prism (light grey lines), and post-prism (medium grey lines) conditions plotted separately for all nine targets. Eye position recordings are synchronized to stimulus onset (vertical dashed line, 1500 ms after trial onset).

significant spatial parameter. These results confirm that the population of neurons in the current study had gain field properties similar to previous publications.

The neural response of 152 (area 7a: 105; area DP: 47) neurons was quantitatively compared during the pre-prism and the prism condition. Of these 152 neurons, 92 (area 7a: 69; area DP: 28) neurons were also analysed during the post-prism condition. In a first step, the neural activity during each epoch in the pre-prism condition was quantified and directly compared to the respective epoch in the prism condition using categorical regressions. Four shift directions were applied: contralateral (left, $n = 14$), ipsilateral (right, $n = 40$), upward ($n = 65$) and downward ($n = 33$). The same categorical regression was utilized for the pre-prism and post-prism comparison. All population analyses were performed separately for areas 7a and DP, and inter-areal differences are reported where appropriate. Responses from an area DP neuron are shown in Fig. 4*A*–*C* and from an area 7a neuron in Fig. 5*A*–*C*. Figure 6 summarizes the percentages of each tuning type for the population of neurons (pre-prism *vs.* prism, Fig. 6*A*; pre-prism *vs.* post-prism, Fig. 6*B*). The different tuning types (C, C×P, NS) were distributed evenly between epochs for all comparisons.

The parameters of the categorical linear regression were further correlated with the behavioural parameters such as RT and MVT, and reach errors (distance of touch end-point from centre of stimulus). All comparisons yielded insignificant correlations with resulting R^2 values less than 0.08. Thus, none of the behavioural measurements had any relationship to the properties of the neuron recorded in that session.

Fixation epoch

Spatially modulated responses before the onset of visual stimulation reflect a pure eye position effect (Bremmer *et al.* 1997). Both sample neurons in the example had weak preferences during the fixation epoch in the pre-prism condition (Figs 4*A* and 5*A*). The DP neuron moved the eye position tuning downward during an upward prism shift (Fig. 4*B* and *D*), and back toward the centre during the post-prism condition (Fig. 4*C* and *E*). The 7a neuron moved the eye position tuning toward the contralateral space during a downward prism shift (Fig. 5*B* and *D*), and toward the centre during the post-prism condition (Fig. 5*C* and *E*). Significant spatial tuning changes between pre-prism and prism condition were observed in 77 neurons (C×P, 51%; Fig. 6*A*). Significant changes in firing rate were observed in 38 of 152 neurons (C, 25%). Thus, significant effects of the prism condition were observed in the majority of neurons (C×P and C, 115 of 152, 76%). The remaining 37 of 152 neurons (24%, type NS) had no effects. After removal of the prism (Fig. 6*B*), neural responses did not return to pre-prism levels and substantial differences in spatial tuning (C×P, 41 of 92, 45%) and firing rate (C, 33 of 92, 36%) remained.

Visual epoch

Significant upper gain field tuning was observed in the DP neuron before the prism perturbation (Fig. 4*A* and *D*). This tuning shifted downward during the prism condition (Fig. 4*B* and *D*). A smaller upward shift occurred after prism removal (Fig. 4*C* and *E*). The 7a neuron showed a

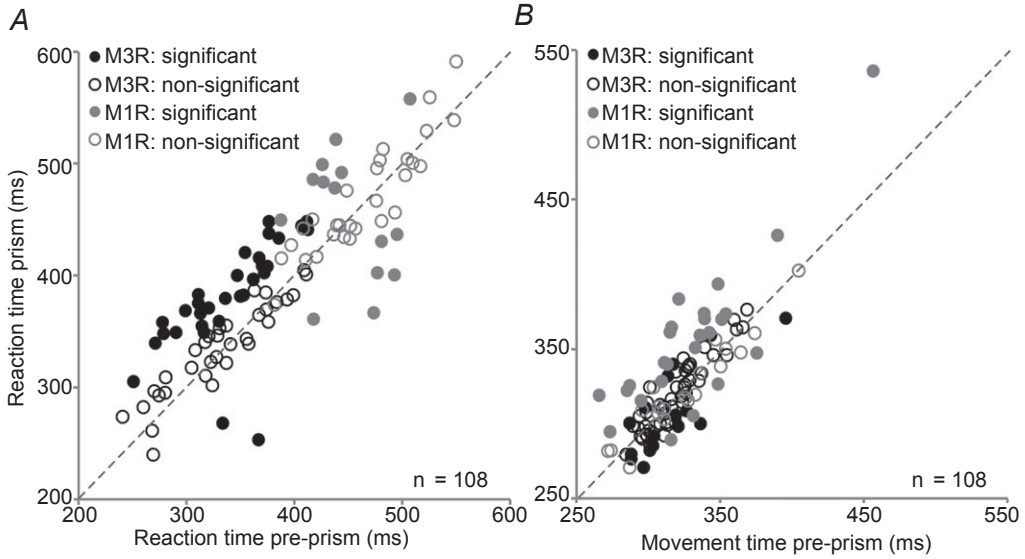

Figure 3. Comparison of mean response times for pre-prism and prism conditions
A, reaction time (time from stimulus change to lift hand). *B*, movement time (time from lift hand to touch). Student's *t test* was used for the comparison between conditions (filled circles, significant; open circles, non-significant) plotted separately for M1R (grey circles) and M3R (black circles).

weak gain field tuning in the pre-prism condition (Fig. 5*A* and *D*). The direction of gain field tuning and overall firing rate changed during the presence of the prism (Fig. 5*B*). Stimuli in the upper and centre eye positions (corresponding to the centre and lower positions without prism) yielded sharp increases in firing rate resulting in a shift of the linear coefficients between pre-prism and prism conditions (Fig. 5*D*). Once the prism was removed, the gain field tuning reversed close to pre-prism levels (Fig. 5*C* and *E*). None the less, the changes in gain field tuning between pre-prism and post-prism conditions were significant for this neuron. For the population of neurons, gain field tuning changed significantly for 44% (C×P, 67 of 152; Fig. 6*A*). An absence of gain field tuning but overall changes in firing rate between conditions was observed in 49 of 152 neurons (C, 32%). These neurons were either not spatially tuned or had large gain fields that extended beyond the display size. Therefore, the majority of neurons (C×P and C combined, 116 of 152, 76%) were affected by the prismatic distortion. The remaining neurons (NS, 36 of 152, 24%) did not show any effects. The pre-prism and post-prism comparison revealed that almost 85% of neurons remained affected by the distortion (C×P, 37 of 92, 40%; C, 41 of 92, 45%; Fig. 6*B*).

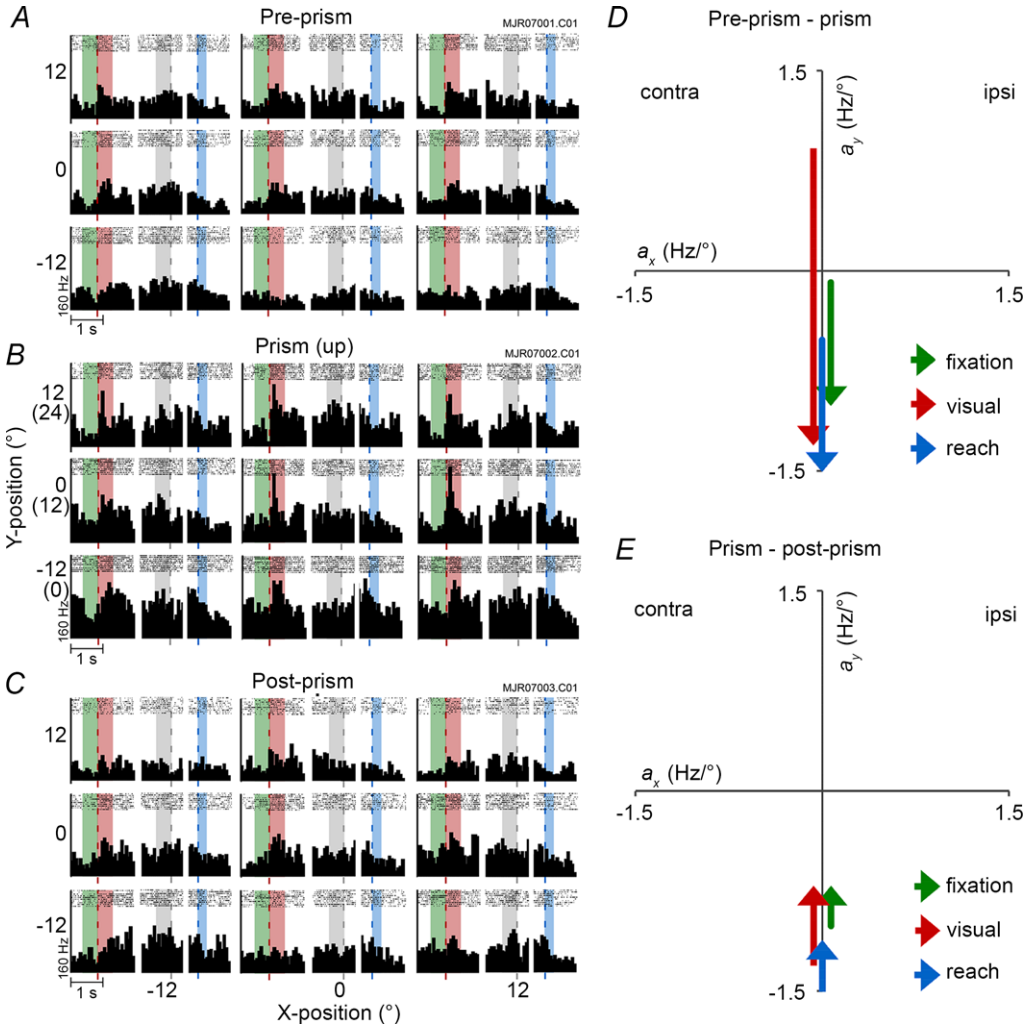

Figure 4. Responses of an area DP neuron (type C×P)
A–C, peri-stimulus time histogram during pre-prism (*A*), prism with 12° upward shift (*B*), and post-prism conditions (*C*). Each peri-stimulus time histogram includes fixation and visual, preparatory and reach epochs averaged over 8–10 trials (bin width 60 ms). They are arranged in a 3 × 3 grid representing each target. *D* and *E*, regression parameters showing the transitions of spatial tuning from pre-prism to prism (*G*) and from prism to post-prism (*H*) conditions plotted separately for each epoch. Fixation: $A_{\text{pre-prism}} = -0.09y + 23$, $A_{\text{prism}} = -1.01y + 52$, $A_{\text{post-prism}} = -0.71y + 28$. Visual: $A_{\text{pre-prism}} = 0.92y + 39$, $A_{\text{prism}} = -1.31y + 88$, $A_{\text{post-prism}} = -0.71y + 44$. Preparatory: $A_{\text{pre-prism}} = 36$, $A_{\text{prism}} = 64$, $A_{\text{post-prism}} = 40$. Reach: $A_{\text{pre-prism}} = -0.52y + 27$, $A_{\text{prism}} = -1.53y + 48$, $A_{\text{post-prism}} = -1.12y + 32$. contra, contralateral; ipsi, ipsilateral.

Preparatory epoch

During this epoch the monkey continued fixating and the hand was resting on the touch sensor. Thus, the overt behaviour and visual stimulation were identical to those of the visual epoch. The DP neuron was not spatially tuned during this epoch but the overall firing rate changed significantly between conditions (Fig. 4*A*–*C*). The 7a unit was weakly spatially tuned and the overall firing rate was low akin to the previous epochs during the pre-prism condition (Fig. 5*A*). During the prism condition the neuron increased its overall firing rate and became strongly spatially tuned for the upper eye positions (Fig. 5*B*). The direction of tuning was similar to the visual epoch but smaller in magnitude (Fig. 5*D*). The neural response reversed back to pre-prism levels once the prism was removed (Fig. 5*C* and *E*). For the population of neurons (Fig. 6*A*), changes in spatial tuning during the preparatory epoch were observed in 67 of 152 neurons (C×P, 44%). About one-third (C, 59 of 152, 38%) were not spatially tuned but changed overall firing rate. Prism effects were therefore observed in the majority of neurons (126 of 152, 83%; C×P and C combined). The remainder (26 of 152; 17%; NS) was not affected by the prism. After prism removal the majority of neurons remained altered (C×P, 37 of 92, 40%; C, 35 of 92, 38%; Fig. 6*B*).

Reach epoch

During the final epoch, the lower eye position tuning of the DP neuron shifted further downward from pre-prism

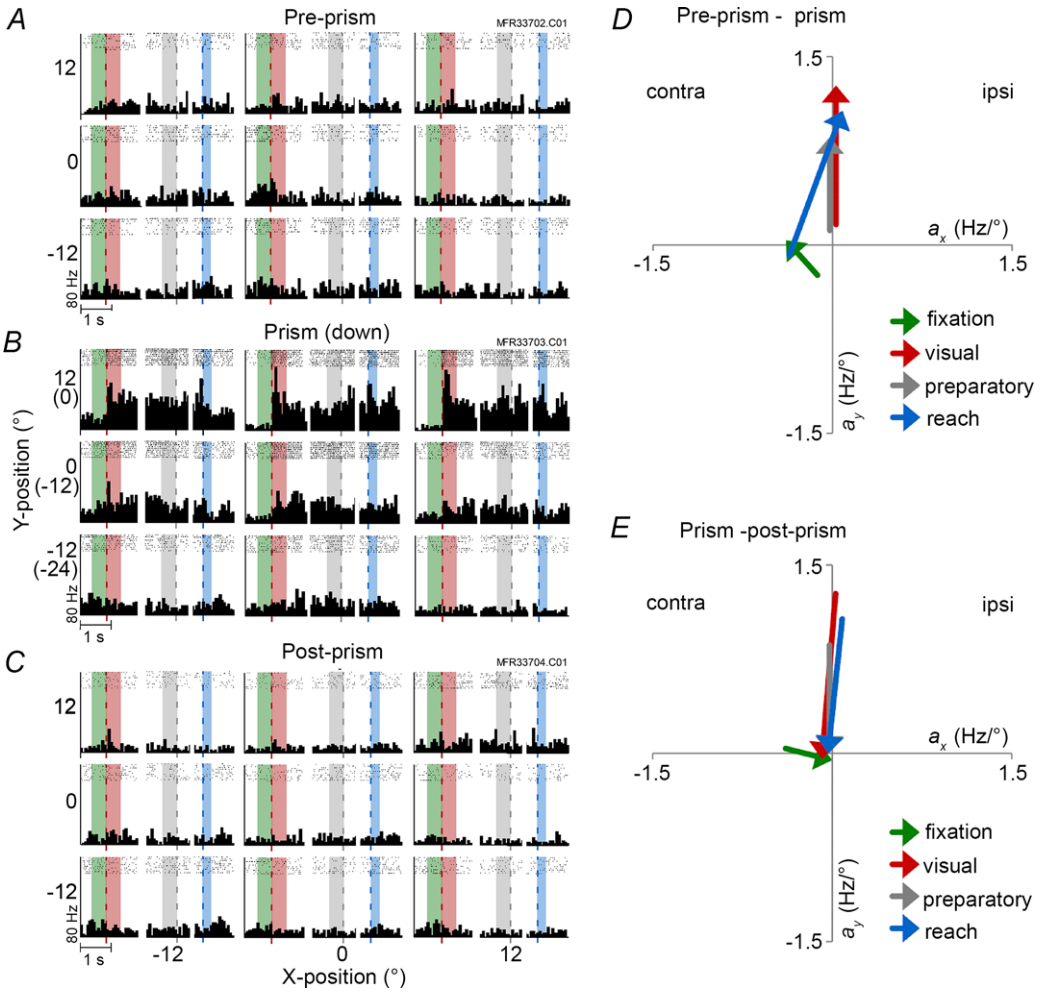

Figure 5. Responses of an area 7a neuron (type C×P)
A–*C*, peri-stimulus time histogram during pre-prism (*A*), prism with 12° downward shift (*B*), and post-prism (*C*) conditions. *D* and *E*, regression parameters from pre-prism to prism (*G*) and from prism to post-prism (*H*) conditions plotted separately for each epoch. Fixation: $A_{pre\text{-}prism} = -0.13x - 0.24y + 11$, $A_{prism} = -0.39x + 0.04y + 11$, $A_{post\text{-}prism} = 0.07x + 7.6$. Visual: $A_{pre\text{-}prism} = 0.16y + 8.6$, $A_{prism} = 1.27y + 35.2$, $A_{post\text{-}prism} = -0.05y + 6.1$. Preparatory: $A_{pre\text{-}prism} = 0.12y + 7.36$, $A_{prism} = 0.86y + 28.9$, $A_{post\text{-}prism} = 0.04y + 6.6$. Reach: $A_{pre\text{-}prism} = -0.36x - 0.08y + 8$, $A_{prism} = 0.08x + 1.07y + 17.8$, $A_{post\text{-}prism} = -0.09y + 5.5$. Conventions are the same as in Fig. 4. contra, contralateral; ipsi, ipsilateral.

to prism condition (Fig. 4*A*, *B* and *D*). After prism removal, the tuning shifted upward again but did not regain pre-prism levels (Fig. 4*C* and *E*). The area 7a neuron was not spatially tuned during the reach epoch under the pre-prism condition (Fig. 5*A*). During the prism condition, the neuron increased its firing rate sharply for reaches made to upper targets (Fig. 5*B*). Although the majority of reach end-points were similar for the pre-prism and the prism conditions, as shown in the behavioural results, the spatial tuning of the neuron differed significantly between the two conditions, as demonstrated by plotting the linear coefficients of the model equations (Fig. 5*D*). Similar to the previous epochs, firing rate and spatial tuning returned close to pre-prism levels once the prism was removed but significant differences lingered (Fig. 5*C* and *E*). The population analysis (Fig. 6*A*) confirmed that significant spatial modulations due to the prism were observed in more than half of the neurons (C×P, 79 of 152, 52%). A smaller proportion of neurons (38 of 152, 25%) were classified as type C neurons. One hundred and seventeen of 152 (C×P and C combined, 77%) neurons were affected by the perceptual distortion. The prisms had no significant effect on 23% of the neurons (NS, 35 of 152). During the reach epoch, the distributions of tuning types differed between areas 7a and DP ($\chi^2 = 6.86$, $P = 0.03$) due to a larger proportion of C×P types in area 7a (59% 7a *vs.* 36% DP). After the prism was removed, the majority of neurons remained altered compared to pre-prism levels (C×P, 42 of 92, 46%; C, 31 of 92, 34%; Fig. 6*B*).

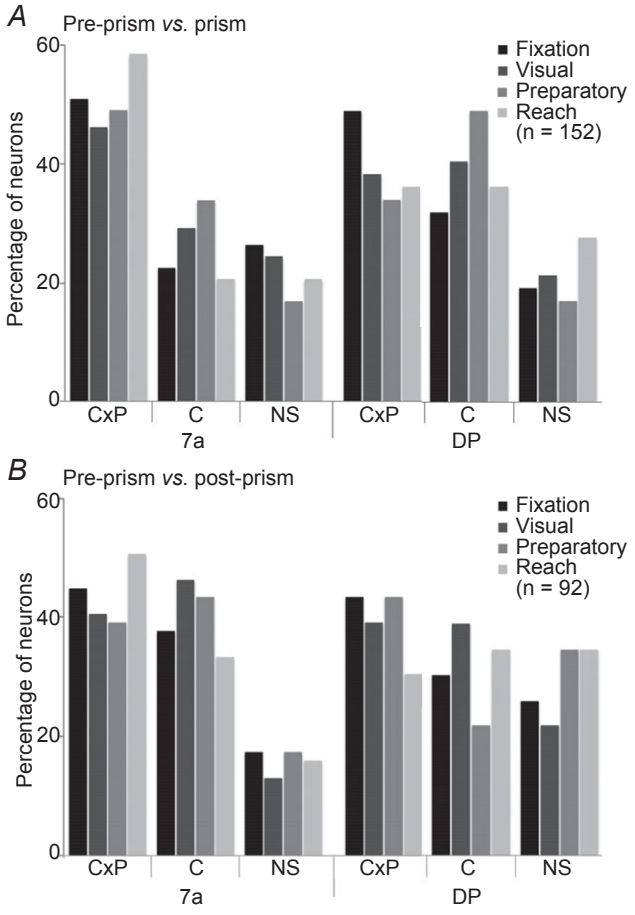

Figure 6. Population distribution of response types
Results from the categorical regression of pre-prism *vs.* prism (*A*) and pre-prism *vs.* post-prism (*B*) comparisons performed separately for each epoch: fixation, visual, preparatory and reach. Proportions of interaction types between C and P are plotted separately for each area (7a *vs.* DP). Type C×P suggests interaction between C and P; these neurons changed spatial tuning between conditions. Type C indicates a single effect of condition; these neurons changed mean firing rate but had no significant spatial tuning. NS cells had no effect of either factor. (type) C, condition; DP, dorsal prelunate; NS, non-significant; (type) P, position.

Combined effects: pre-prism, prism and post-prism conditions

If the spatial tuning and firing rate completely reversed to pre-prism levels after removal of the prism, we should not expect any condition effects, that is, an absence of tuning types C and C×P in the pre-prism *vs.* post-prism comparison. This was not the case and strong post-prism effects lingered in the population of neurons (Fig. 6*B*). However, the proportions of C and C×P types significantly decreased between the two comparisons (between pre-prism *vs.* post-prism and pre-prism *vs.* post-prism) in area 7a when data for all epochs were combined ($\chi^2 = 15.78$, $P = 0.0004$).

As most neurons altered their firing rate between conditions (between 55 and 70% across all epochs, C and some C×P types), the average changes in intercept were assessed between the following three comparisons: prism *vs.* pre-prism, post-prism *vs.* pre-prism, and control2 *vs.* control1. Overall, this comparison yielded highly significant differences ($F_{2,656} = 16.74$, $P < 0.0001$). The greatest intercept changes were observed between prism *vs.* pre-prism and control2 *vs.* control1 ($P = 0.0005$, Tukey's HSD) and between prism *vs.* pre-prism and post-prism *vs.* pre-prism ($P < 0.0001$, Tukey's HSD). These neurons were grouped into cells with either significant increases or decreases in firing rate. Between pre-prism and prism conditions for all epochs combined, an average of 32% of area 7a neurons and 41% of area DP neurons had significant increases in firing rate, while 31% of area 7a neurons and 20% of DP neurons decreased their firing rate. Between pre-prism and post-prism conditions, the percentage of neurons with positive changes dropped to 24% for area 7a and 31% for area DP. The percentage of neurons with significant decreases in firing rate was 41% in area 7a and 19% in area DP. Only a small proportion of neurons had significant increases in firing rate when

comparing the two control conditions (0% in area 7a, 15% in area DP). Significant decreases were observed in 23% of neurons in both areas, while more than two-thirds of neurons had no changes. In the next step, the relationship between direction of prism shift and changes in spatial tuning was examined for the population of C×P type neurons.

Modulation of eye position tuning due to displacement of the perceived visual field. ***Population angular tuning.*** The spatial aspects of the neural response during the pre-prism and prism conditions were further analysed by comparing the linear coefficients and angular tuning of the C×P type neurons. The sample neurons both illustrate cases where the induced shift in spatial tuning occurred along the axis of prism distortion (vertical). The population eye position tuning during all three conditions was further evaluated for C×P neurons separately for each area. The tuning during each of the four epochs was analysed with circular statistics. For all epochs, the angles were distributed uniformly during the pre-prism, prism and post-prism conditions, as confirmed by the Hotelling test. This matches our previous study, which showed a uniform distribution of angles during the four measurement epochs. The difference vectors between prism and pre-prism conditions were distributed uniformly indicating that there were no systematic shifts of spatial tuning in the population of neurons. The pre-prism *vs.* post-prism comparison yielded a uniform distribution of difference vectors. The amplitude of these difference vectors was further evaluated for all three combinations: prism–pre-prism, post-prism–pre-prism and control2–control1. Overall, this comparison yielded highly significant effects ($F_{2,491} = 9.25$, $P = 0.0001$). Significant changes in vector amplitude were observed for the prism–pre-prism *vs.* control2–control1 comparison ($P = 0.0015$, Tukey's HSD) as well as for the prism–pre-prism *vs.* post-prism–pre-prism comparison ($P = 0.004$, Tukey's HSD). The difference vectors between pre-prism and prism conditions were about twice as large as between the two control conditions.

The changes in spatial tuning for each of the four epochs (fixation, visual, preparatory and reach) were further assessed with respect to the direction of prism displacement. The main finding was that for the population of neurons there was no systematic relationship between the direction of distortion and the direction of tuning shift. To further analyse this relationship, neurons were classified into three different groups. (1) *Matching*: Spatial tuning altered in the same direction as the prism distortion (angle difference <45°). For example, the prism shifted the visual field to the ipsilateral space and the spatial tuning changed in the same direction (i.e. increasing horizontal coefficient). Such congruence between spatial tuning and prism shift occurred in 28% of the C×P neurons (fixation 36%; visual preparatory, and reach epochs each 25%). (2) *Orthogonal*: Spatial tuning changed orthogonal to the induced prism distortion (angle difference ≥45° and <135°). For example, when the prism distorted the visual field upwards the spatial tuning shifted along the horizontal axis. Orthogonal tuning changes were demonstrated by 42% of the C×P neurons (fixation 44%; visual 37%; preparatory 42%; and reach epoch 45%). (3) *Opposite*: Spatial tuning altered in the opposite direction of the prism distortion (angle difference ≥135° and <225°). For example, the prism distorted the visual field into the ipsilateral space but the spatial tuning shifted towards the contralateral side (i.e. decreasing horizontal coefficient). Such an opposite shift was observed in 30% of the C×P neurons (fixation 20%; visual 37%; preparatory 33%; and reach epoch 29%). The neurons illustrated in Figs 4 and 5 fall into this category. These analyses show that for the majority of neurons, spatial tuning did not systematically follow the direction of the prism distortion. For a given prism shift, the gain field tuning of area 7a and DP neurons altered in variable directions. To further analyse these transformations between the two gain fields more systematically we calculated Euler angles and translation.

Remapping of spatial tuning (transformation analysis). Each neuron's gain field can be modelled as a plane in 3D space with x and y as the spatial parameters and z as the firing rate for the 0°, 0° position derived from the linear regression (see Heider *et al.* 2010*a*, Figs 6 and 8). Each epoch was defined as a neural state, where any position in this 3D space is a triad (x, y and firing rate z). Under this assumption, we found a transformation with rotation and translation operators that describe the change between conditions. Thus, for each C×P type neuron, we calculated the rotation and translation between pre-prism and prism, as well as between pre-prism and post-prism conditions. The rotation transformation in Euler angles was plotted separately for both comparisons, (pre-prism *vs.* prism and pre-prism *vs.* post-prism, Fig. 7*A, B*). Only the α (x-axis) and β (y-axis) angles are presented because these are related to the spatial coordinates in contrast to the γ (z-axis) angle, which is related to the firing rate. For the population of neurons in areas 7a and DP, α and β angles approximate a sinusoidal function with a small phase shift and amplitude that was similar for all epochs. The sinusoidal functions are indistinguishable between areas. To fit these functions we had to combine all four directions of prism shift (0°, 90°, 180° and 270°). In turn, the x and y components of the translation showed a negative relation, that is, crossing close to the centre location (0°, 0°) for all epochs (Fig. 8*A* and *B*). This means that

when there was a positive displacement on the *x*-axis there was a negative displacement along the *y*-axis and *vice versa*. The magnitude of these translation effects sometimes exceeded the vertical and horizontal dimensions of the display (−18° and 18°). An alternative interpretation for the rotational matrix is to use a unitary vector ($\hat{\mathbf{e}}$) and an angle (θ) of revolution around the vector $\hat{\mathbf{e}}$, also referred to as *angle-axis representation*. The population analysis showed that neurons in areas 7a and DP followed a similar trend for the pre-prism *vs.* prism and for the pre-prism *vs.* post-prism comparison (Fig. 9*A* and *B*). When plotting $\hat{\mathbf{e}}_x$ and $\hat{\mathbf{e}}_y$ (*x* and *y* component of $\hat{\mathbf{e}}$) two clusters emerged in the upper right and lower left quadrants. The mean for each cluster was calculated, and a line was drawn from the origin (0,0) to the mean of each cluster. It is apparent that the two clusters can be aligned with a straight line at a 45° angle from the *x*-axis generating a continuous line.

Discussion

The current study demonstrates that spatially tuned activity of area 7a and DP neurons was strongly affected by prismatic distortion during a VGR task. Behaviourally, the perceptual distortion caused a shift in eye position and created a mismatch between the perceived and actual reach target locations. In terms of spatial representation, the prism induced a misalignment of eye and hand centred reference frames. Human imaging studies demonstrate that the recalibration required for successful reaching to the actual target is accompanied by increasing haemodynamic activation in the parietal cortex (Clower *et al.* 1996; Danckert *et al.* 2008; Luauté *et al.* 2009). Neurological patients with PPC lesions are impaired in this recalibration process (Gréa *et al.* 2002; Newport & Jackson, 2006). These findings have been attributed to a crucial role of the PPC for online error correction

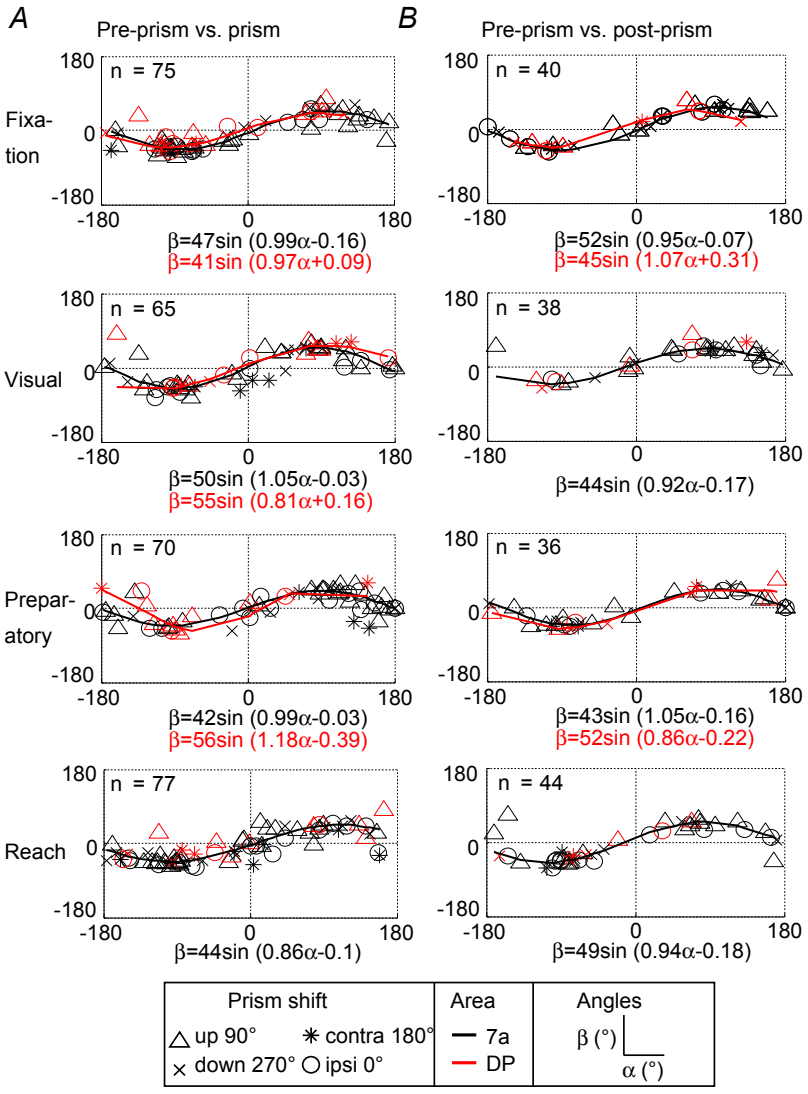

Figure 7. Angular Euler representation of prism distortion on spatial response fields
A, transformation from pre-prism to prism condition. *B*, transformation from pre-prism to post-prism condition. *X*-axis (α) *vs.* *Y*-axis (β) rotation for all epochs separated by area (7a and DP) and by direction of prism distortion (upward = 90°, downward = 270°, ipsi = 0°, contra = 180°). A sinus function is fit to the angles in those subpopulations where the goodness of fit was $R^2 \geq 0.5$. contra, contralateral; DP, dorsal prelunate; ipsi, ipsilateral.

during reaching, which relies on a combination of visual, proprioceptive and efference copy signals (Della-Maggiore *et al.* 2004). In non-human primates, prism studies have focused on electrophysiological recordings from premotor cortex (Kurata & Hoshi, 1999, 2002), primary visual cortex (Sugita, 1996) or cerebellum (Baizer *et al.* 1999). Earlier studies in the PPC have utilized prisms during gain field tasks without reaching and found that by deviating the eye position, the gain field tuning of area 7a neurons was the same as by changing the position of the fixation target (Andersen *et al.* 1985, 1987). However, little is known about how these neurons respond to a perceptual perturbation when the animal has to touch the displaced stimulus under visual guidance. We hypothesized that PPC neurons would recalibrate their spatial representation to accommodate the distortion.

Behavioural effects of prismatic distortion

Rapid improvement in reach accuracy occurred within a few trials even with limited visual feedback and matches human psychophysical findings (Rossetti *et al.* 1993; Clower & Boussaoud, 2000; Fernandez-Ruiz *et al.* 2006; Lee & van Donkelaar, 2006). One important question is how much of the adaptation is due to the induced change in eye position or whether it is directly generated by the mismatch between visual and proprioceptive signals, and how that affects the reach performance. Transfer from oculomotor to the manual system has been reported previously in the context of saccade adaptation (Cotti *et al.* 2007). However, saccadic adaptation in trained human subjects takes about 20 trials (Awater *et al.* 2005), and thus operates over larger time scales. Unlike saccadic adaptation, prism adaptation occurs once feedback from the mismatched hand location becomes available at the end of the reach movement (Redding & Wallace, 2000). Prism adaptation also depends on the error between perceived target position and the reach end-point (Clower & Boussaoud, 2000; Norris *et al.* 2001), as proposed by a linear dynamical model system (Cheng & Sabes, 2007). By receiving visual feedback at the end of every trial,

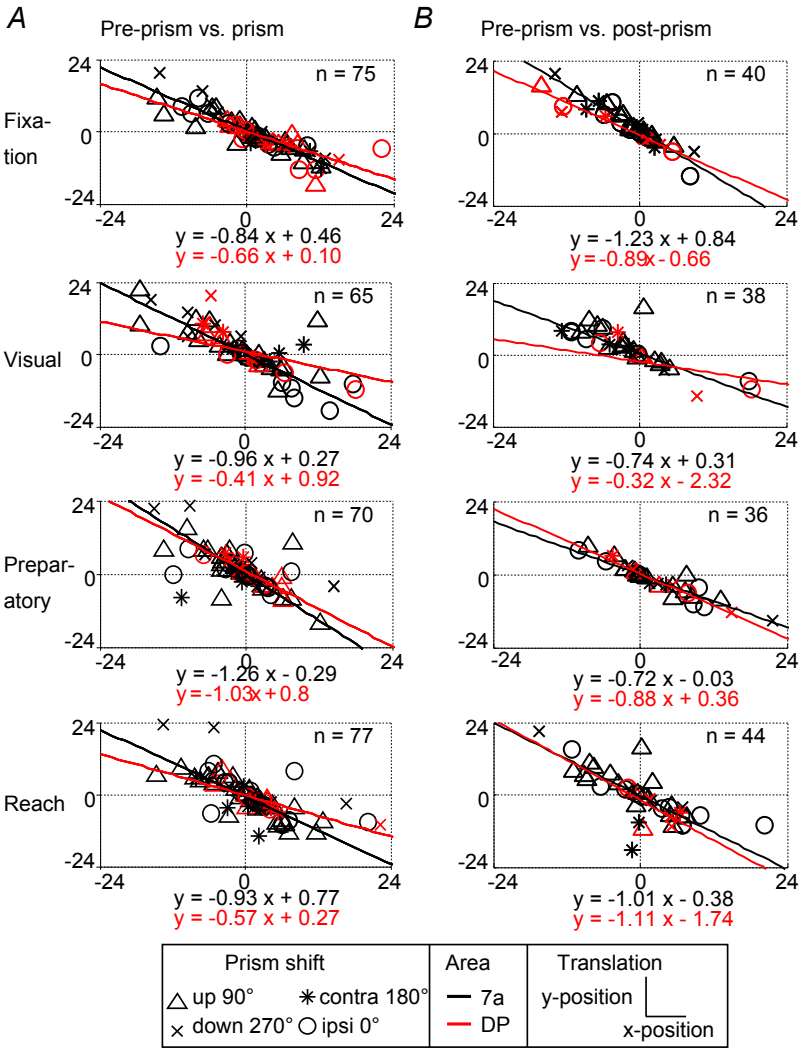

Figure 8. Translation of spatial response fields with prism distortion
A, transformation from pre-prism to prism condition. *B*, transformation from pre-prism to post-prism condition. Displacement space representation and fits for all epochs separated by area (7a and DP) and by direction of prism distortion (upward = 90°, downward = 270°, ipsi = 0°, contra = 180°). contra, contralateral; DP, dorsal prelunate; ipsi, ipsilateral.

the reach is perceptually calibrated within a few trials. The precise neural mechanisms underlying these adaptive processes are not yet fully understood. Studies in parietal area V6A demonstrate a strong effect of visual feedback during movement-related neural activity, suggesting that these neurons might play a critical role in monitoring and correcting motor actions (Bosco *et al.* 2010).

Neural modulation due to prismatic distortion

In a previous study (Heider *et al.* 2010*a*), we demonstrated that the majority of area 7a and DP neurons modulated their neural activity during the course of a VGR task despite constant visual stimulation. Thus, gain field and retinotopic tuning is far from static in these areas. Similarly, findings in the dorsal premotor (PMd) and motor (M_1) cortex demonstrated that spatial tuning during the preparatory phase does not necessarily match that of the movement phase (Churchland *et al.* 2010). These signatures of sensorimotor transformation have been demonstrated in different areas of the parietal cortex (Burnod *et al.* 1999; Battaglia-Mayer *et al.* 2000; Buneo *et al.* 2002; Fattori *et al.* 2005; Chang & Snyder, 2010). As the PPC neurons receive multisensory inputs and connect to multiple cortical areas (Lewis & Van Essen, 2000; Stepniewska *et al.* 2005; Rozzi *et al.* 2006), their neural properties are susceptible to changes in visual and behavioural parameters. Thus, any form of perturbation will probably require additional computations to correct for the mismatch (Diedrichsen *et al.* 2005; Chang *et al.* 2009).

In the current study, the prismatic distortion caused two forms of neural changes. First, more than half of all neurons showed significant increases or decreases in average firing rate. Second, almost half of all neurons altered their gain field tuning, that is, the modelled spatial parameters changed between pre-prism and prism conditions. If spiking activity of PPC neurons were

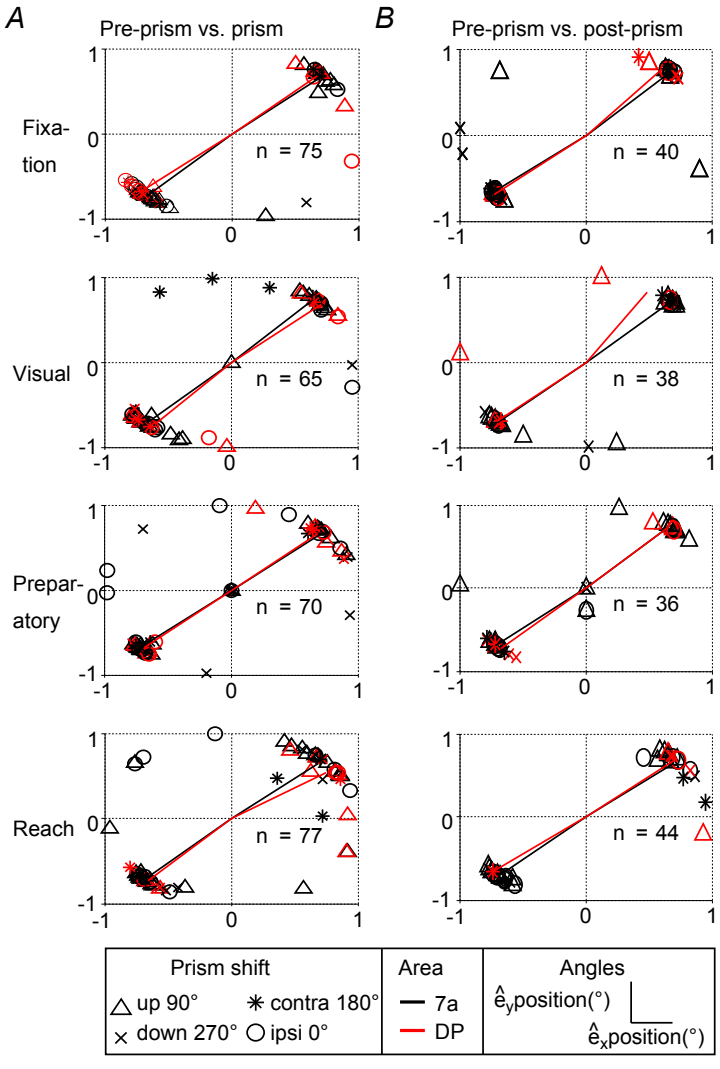

Figure 9. Angle–axis representation of spatial response fields with prism distortion
A, transformation from pre-prism to prism condition. *B*, transformation from pre-prism to post-prism condition. Plotted are $\hat{e}_x$ and $\hat{e}_y$ spatial coordinates of the unit vector for all epochs separated by area (7a and DP) and by direction of prism distortion (upward = 90°, downward = 270°, ipsi = 0°, contra = 180°). Lines are plotted from the origin (0°, 0°) to the mean position of each cluster separately for each area (7a and DP). contra, contralateral; DP, dorsal prelunate; ipsi, ipsilateral.

determined solely by eye position or visual stimulation, minimal changes should emerge at least during the early phases of the task when fixation spot and visual target are simply shifted by the prism. For example, a neuron with an upper gain field tuning should retain its preference if the eyes simply move up or down during the prism exposure and the resulting vertical linear coefficients should remain constant. This behaviour resembles that of the type V cells described in the ventral premotor area during prismatic distortion (Kurata & Hoshi, 2002). However, substantial modulation occurred during all phases of the task in the recorded population of PPC neurons. This modulation could be due to the incongruence between eye position and final reach position. We found that the deviation of the eye positions were fairly small and could not account for the drastic changes in tuning. The visual perturbation had a mixed influence on the eye position tuning and did not follow a strict visual or motor co-ordinate system. This suggests that the prism caused more generalized effects that did not directly correlate with the direction of the visual shifts.

Increased attentional demands probably contributed to the changes in neural activity but the degree of such attentional modulation remains uncertain. In V6A, a reaching area located in the medial PPC, modulations from spatially shifting covert attention were observed in about half of the tested cells suggesting that spatial attention is linked to motor planning (Galletti *et al.* 2010). This study also found that the spatial preference of the attentional modulation did not necessarily match that of the retinotopic tuning. In two other areas of the PPC, the 'parietal reach region' (PRR) and lateral intraparietal area, neural activity is more predictive of movement planning than attention alone (Quian Quiroga *et al.* 2006). This suggests that spatially tuned activity during the delay phase of a reaching task is not driven by spatial attention alone. However, the influence of attention might be higher in areas 7a and DP. Neurons in area 7a have been shown to alter their retinotopic tuning due to changed attentional demands (Steinmetz *et al.* 1994; Quraishi *et al.* 2007). Thus, changes in spatial tuning may be partially due to shifts in the locus of spatial attention.

If a reach movement is planned to a location that is systematically offset from the eye position, additional computations are required during the planning phase. Studies analysing neural response latencies indicate that this planning process originates in the frontal cortex and is relayed to the parietal areas via corollary discharge (Johnson *et al.* 1996; Westendorff *et al.* 2010). Temporal comparison between the PRR and PMd suggests that activity in the PRR 'fine-tunes' the reach plan (Johnson & Ferraina, 1996; Boussaoud & Bremmer, 1999). Neural modulations in areas 7a and DP could reflect adaptive fine-tuning of the reach plan under the prism condition.

Substantial changes of neural activity were not only observed during the prism exposure but also during the post-prism condition suggesting pervasive and long-lasting neural effects of the perturbation. Studies in the cortical motor areas and parietal area 5 demonstrate that force-field perturbations or changes in arm orientation induce consistent and prolonged changes in spatial tuning and average firing rate of single neurons (Scott & Kalaska, 1997; Scott *et al.* 1997; Li *et al.* 2001; Padoa-Schioppa *et al.* 2004). These findings suggest that in motor and premotor areas, neural responses are highly susceptible to task perturbations. Dynamic changes in neural properties were also present when the same task was repeated without any perturbations (Padoa-Schioppa *et al.* 2004; Rokni *et al.* 2007). Such long-lasting effects in the absence of perturbation are believed to originate from network changes (Li *et al.* 2001). Rokni *et al.* (2007) proposed that dynamic response patterns arise from changes in synaptic inputs and that any given behaviour can be realized by multiple configurations of synaptic strengths (Kalaska & Green, 2007). Thus, the same behavioural goal can be achieved by different network patterns and relative contribution of individual neuron activity, which is relevant for the design of reliable brain–computer interfaces (Carmena *et al.* 2005).

Unlike neurons in primary sensory areas, for example in area V1 (Gur & Snodderly, 2006), the PPC neurons are more variable in their firing patterns (Falkner *et al.* 2013). It is intuitive to assume that repeated behaviour results in invariable visuomotor spatial maps, based on the assumption that similar behaviours require similar neural networks. A change in behavioural pattern on the other hand recruits different neural networks resulting in different neural responses. A study in the PMd and primary motor cortex confirmed that the relationship between practised behaviour and neural activity is reasonably stable over time (Chestek *et al.* 2007). Even though the monkeys were over-trained for the reaching task in the current study, the performance was seldom static; the reach end-point locations varied between trials. Although these minor changes in behaviour were within the permitted error range to complete the task correctly, they probably affected the neural response, as shown by Chestek *et al.* (2007). The changes in tuning properties of neurons in areas 7a and DP observed during the prism distortion were about three times larger than those observed during mere repetition. The observed changes are therefore not simply a result of change in motivation or attention but also result from the interaction with extrapersonal space perturbed by the prism shift.

Spontaneous ongoing activity without sensory stimulation constitutes a large component of neural modulations in awake, adult animals (Fiser *et al.* 2004; Petermann *et al.* 2009; Destexhe, 2011) and probably contributes to the changes observed during the control

experiments. We propose that any perturbation strongly modulates these internal (ongoing) processes, and that these modulations last beyond the actual exposure. The actual sensory changes invoked by the prism played a minor role in altering neural responses. Instead, the prisms altered ongoing network fluctuations and in turn triggered the dramatic changes in overall firing rate and spatial tuning. The transformation analysis further showed that these network changes did not follow a random pattern.

Spatial transformations during prismatic adaptation

Gain field tuning changes between pre-prism and prism condition were uniformly distributed for each epoch and area. Furthermore, angular distributions of difference vectors did not correlate with the direction of the applied prismatic shift. However, the transformation analysis of the gain fields between conditions suggests that the observed spatial changes were not randomly distributed, but rather showed a systematic relationship for the horizontal and vertical (α and β) components of the Euler rotation, and the x and y components of the translation, which were similar for both areas and all analysis epochs.

Rotation. There was a systematic relationship between the α and β components following a sinusoidal function. The full range of angles was represented indicating that spatial transitions of some neurons moved clockwise while others moved counter-clockwise. Neurons close to either end of the sinusoid ($\pm$180°, 0°) overturned their response fields by approximately 180°, whereas neurons located close to the centre (0°, 0°) had minimal rotation of their response fields. A high concentration of neurons had rotation angles around 90°, 90° and −90°, −90°; thus these neurons rotated their gain fields approximately at right angles. Basic functions (e.g. sine, cosine, Gaussian) have been proposed previously for sensory motor transformations (Pouget & Sejnowski, 1997). The angle-axis representation indicates that the majority of neurons preserved a common axis of rotation, which is remarkable for multiple reasons: First, all neurons started with diverse gain fields during the pre-prism condition. Second, four different directions of prism shift were applied, which were often not aligned with the main axis of gain field tuning. Third, the angle-axis measurements were similar for all four epochs. Fourth, all recordings were accumulated from single penetrations over several months in each monkey. Thus, the angle-axis properties were not a transient property arising from simultaneous recordings, for example, those obtained with arrays (Churchland *et al.* 2010). Fifth, neurons were sampled from two areas, which have similar gain field properties during reaching (Heider *et al.* 2010*a*). Sixth, both comparisons (pre-prism *vs.* prism and pre-prism *vs.* post-prism) yielded very similar angle-axis results.

Translation. A large proportion of spatially tuned neurons shifted their gain fields suggesting remapping of the spatial representation (Wang & Sainburg, 2005). The prism itself translated the visual space by a constant amount. None the less, the translation amplitude, as modelled by the analysis, varied substantially between neurons. For the population of neurons, the translation coefficients followed a constant slope between x and y, and were not distributed randomly.

The regular transformations confirm that these spatially tuned neurons achieve to preserve a stable internal representation, which can then be used as output for target neurons in projection areas, for example in the frontal cortex (Johnson *et al.* 1996; Rozzi *et al.* 2006; Beurze *et al.* 2007). These findings also suggest that PPC neurons combine different spatial representations (e.g. gain field, retinotopy, spatial attention) into a more abstract representation where the different signals are combined in a non-linear way (Pouget & Sejnowski, 1997). This network behaviour cannot be demonstrated at the single cell level. In our case, about 70 neurons were sufficient to demonstrate these network effects. We further hypothesize that this network behaviour requires sampling across a larger area of cortex (i.e. several millimetres) possibly across many cortical columns. To create such systematic transformations, neurons require an error signal from the reach movement under the distorted condition. Thus, direct interaction with the environment steadily remaps the spatial representation between conditions. A variety of signals are therefore needed for this remapping process. Continuous updating of eye-centred representations after head and eye movements has been described previously (Batista *et al.* 1999; Pouget *et al.* 2002). When presented with the prism distortion, corollary discharge from the reaching limb and the eyes is combined with the visual cue to aid in short-term reorganization of spatial representation (Fernandez-Ruiz *et al.* 2006). We hypothesize that the translation of gain fields largely reflects altered *inputs* from sensory (e.g. visual or proprioceptive) and other sources (e.g. efference copy) derived from the error signals during reaching. The systematic distribution of rotations, as confirmed by the angle-axis representation, reflects the *output* of area 7a and DP neurons. Such systematic output is reminiscent of the concept of 'labelled lines' where specific neural elements transmit a constant signal to the next cortical areas, except in our case the transmission corresponds to a specific network pattern. Reaching studies in humans suggest that adaptation to novel conditions creates remapping between target vectors and movement vectors and thus permits generalization across conditions (Messier & Kalaska, 1999; Wang & Sainburg, 2005). Our findings point to a dynamic remapping of spatial transformations while preserving a constant representation of these changes, which in turn enables maintaining the alignment to the outside world.

References

Andersen RA & Mountcastle VB (1983). The influence of the angle of gaze upon the excitability of the light-sensitive neurons of the posterior parietal cortex. *J Neurosci* **3**, 532–548.

Andersen RA, Essick GK & Siegel RM (1985). Encoding of spatial location by posterior parietal neurons. *Science* **230**, 456–458.

Andersen RA, Essick GK & Siegel RM (1987). Neurons of area 7 activated by both visual stimuli and oculomotor behavior. *Exp Brain Res* **67**, 316–322.

Andersen RA, Asanuma C, Essick G & Siegel RM (1990). Corticocortical connections of anatomically and physiologically defined subdivisions within the inferior parietal lobule. *J Comp Neurol* **296**, 65–113.

Arieli A, Grinvald A & Slovin H (2002). Dural substitute for long-term imaging of cortical activity in behaving monkeys and its clinical implications. *J Neurosci Methods* **114**, 119–133.

Awater H, Burr D, Lappe M, Morrone MC & Goldberg ME (2005). Effect of saccadic adaptation on localization of visual targets. *J Neurophysiol* **93**, 3605–3614.

Baizer JS, Kralj-Hans I & Glickstein M (1999). Cerebellar lesions and prism adaptation in Macaque monkeys. *J Neurophysiol* **81**, 1960–1965.

Batista AP & Andersen RA (2001). The parietal reach region codes the next planned movement in a sequential reach task. *J Neurophysiol* **85**, 539–544.

Batista AP, Buneo CA, Snyder LH & Andersen RA (1999). Reach plans in eye-centered coordinates. *Science* **285**, 257–260.

Batschelet E (1981). *Circular Statistics in Biology*. Academic Press, London.

Battaglia-Mayer A, Ferraina S, Mitsuda T, Marconi B, Genovesio A, Onorati P, Lacquaniti F & Caminiti R (2000). Early coding of reaching in the parietooccipital cortex. *J Neurophysiol* **83**, 2374–2391.

Battaglia-Mayer A, Mascaro M, Brunamonti E & Caminiti R (2005). The over-representation of contralateral space in parietal cortex: a positive image of directional motor components of neglect? *Cereb Cortex* **15**, 514–525.

Battaglia-Mayer A, Mascaro M & Caminiti R (2007). Temporal evolution and strength of neural activity in parietal cortex during eye and hand movements. *Cereb Cortex* **17**, 1350–1363.

Beurze SM, de Lange FP, Toni I & Medendorp WP (2007). Integration of target and effector information in the human brain during reach planning. *J Neurophysiol* **97**, 188–199.

Bosco A, Breveglieri R, Chinellato E, Galletti C & Fattori P (2010). Reaching activity in the medial posterior parietal cortex of monkeys is modulated by visual feedback. *J Neurosci* **30**, 14773–14785.

Boussaoud D & Bremmer F (1999). Gaze effects in the cerebral cortex: reference frames for space coding and action. *Exp Brain Res* **128**, 170–180.

Bremmer F, Distler C & Hoffmann KP (1997). Eye position effects in monkey cortex. II. Pursuit- and fixation-related activity in posterior parietal areas LIP and 7A. *J Neurophysiol* **77**, 962–977.

Buneo CA, Jarvis MR, Batista AP & Andersen RA (2002). Direct visuomotor transformations for reaching. *Nature* **416**, 632–636.

Burnod Y, Baraduc P, Battaglia-Mayer A, Guigon E, Koechlin E, Ferraina S, Lacquaniti F & Caminiti R (1999). Parieto-frontal coding of reaching: an integrated framework. *Exp Brain Res* **129**, 325–346.

Carmena JM, Lebedev MA, Henriquez CS & Nicolelis MAL (2005). Stable ensemble performance with single-neuron variability during reaching movements in primates. *J Neurosci* **25**, 10712–10716.

Caselli P, Conforto S, Schmid M, Accornero N & D'Alessio T (2006). Difference in sensorimotor adaptation to horizontal and vertical mirror distortions during ballistic arm movements. *Hum Mov Sci* **25**, 310–325.

Chang SWC & Snyder LH (2010). Idiosyncratic and systematic aspects of spatial representations in the macaque parietal cortex. *Proc Natl Acad Sci U S A* **107**, 7951–7956.

Chang SWC, Papadimitriou C & Snyder LH (2009). Using a compound gain field to compute a reach plan. *Neuron* **64**, 744–755.

Cheng S & Sabes PN (2007). Calibration of visually guided reaching is driven by error-corrective learning and internal dynamics. *J Neurophysiol* **97**, 3057–3069.

Chestek CA, Batista AP, Santhanam G, Yu BM, Afshar A, Cunningham JP, Gilja V, Ryu SI, Churchland MM & Shenoy KV (2007). Single-neuron stability during repeated reaching in Macaque premotor cortex. *J Neurosci* **27**, 10742–10750.

Christel MI & Billard A (2002). Comparison between macaques' and humans' kinematics of prehension: the role of morphological differences and control mechanisms. *Beh Brain Res* **131**, 169–184.

Churchland MM, Cunningham JP, Kaufman MT, Ryu SI & Shenoy KV (2010). Cortical preparatory activity: Representation of movement or first cog in a dynamical machine? *Neuron* **68**, 387–400.

Clower DM & Boussaoud D (2000). Selective use of perceptual recalibration versus visuomotor skill acquisition. *J Neurophysiol* **84**, 2703–2708.

Clower DM, Hoffman JM, Votaw JR, Faber TL, Woods RP & Alexander GE (1996). Role of posterior parietal cortex in the recalibration of visually guided reaching. *Nature* **383**, 618–621.

Cotti J, Guillaume A, Alahyane N, Pelisson D & Vercher J-L (2007). Adaptation of voluntary saccades, but not of reactive saccades, transfers to hand pointing movements. *J Neurophysiol* **98**, 602–612.

Cressman EK & Henriques DYP (2009). Sensory recalibration of hand position following visuomotor adaptation. *J Neurophysiol* **102**, 3505–3518.

Danckert J, Ferber S & Goodale MA (2008). Direct effects of prismatic lenses on visuomotor control: an event-related functional MRI study. *Eur J Neurosci* **28**, 1696–1704.

Della-Maggiore V, Malfait N, Ostry DJ & Paus T (2004). Stimulation of the posterior parietal cortex interferes with arm trajectory adjustments during the learning of new dynamics. *J Neurosci* **24**, 9971–9976.

Desmurget M, Turner RS, Prablanc C, Russo GS, Alexander GE & Grafton ST (2005). Updating target location at the end of an orienting saccade affects the characteristics of simple point-to-point movements. *J Exp Psychol Hum Percept Perform* **31**, 1510–1536.

Destexhe A (2011). Intracellular and computational evidence for a dominant role of internal network activity in cortical computations. *Curr Opin Neurobiol* **21**, 717–725.

Diedrichsen J, Hashambhoy Y, Rane T & Shadmehr R (2005). Neural correlates of reach errors. *J Neurosci* **25**, 9919–9931.

Falkner AL, Goldberg ME & Krishna BS (2013). Spatial representation and cognitive modulation of response variability in the lateral intraparietal area priority map. *J Neurosci* **33**, 16117–16130.

Fattori P, Kutz DF, Breveglieri R, Marzocchi N & Galletti C (2005). Spatial tuning of reaching activity in the medial parieto-occipital cortex (area V6A) of macaque monkey. *Eur J Neurosci* **22**, 956–972.

Fernandez-Ruiz J, Diaz R, Moreno-Briseno P, Campos-Romo A & Ojeda R (2006). Rapid topographical plasticity of the visuomotor spatial transformation. *J Neurosci* **26**, 1986–1990.

Fiser J, Chiayu C & Weliky M (2004). Small modulation of ongoing cortical dynamics by sensory input during natural vision. *Nature* **431**, 573–578.

Galletti C, Battaglini PP & Fattori P (1995). Eye position influence on the parieto-occipital area PO (V6) of the macaque monkey. *Eur J Neurosci* **7**, 2486–2501.

Galletti C, Breveglieri R, Lappe M, Bosco A, Ciavarro M & Fattori P (2010). Covert shift of attention modulates the ongoing neural activity in a reaching area of the Macaque dorsomedial visual stream. *PLoS One* **5**, e15078.

Gréa H, Pisella L, Rossetti Y, Desmurget M, Tilikete C, Grafton S, Prablanc C & Vighetto A (2002). A lesion of the posterior parietal cortex disrupts on-line adjustments during aiming movements. *Neuropsychologia* **40**, 2471–2480.

Gur M & Snodderly DM (2006). high response reliability of neurons in primary visual cortex (V1) of alert, trained monkeys. *Cereb Cortex* **16**, 888–895.

Hadjidimitrakis K, Bertozzi F, Breveglieri R, Fattori P & Galletti C (2013). Body-centered, mixed, but not hand-centered coding of visual targets in the medial posterior parietal cortex during reaches in 3D space. *Cereb Cortex* doi: 10.1093/cercor/bht181.

Heider B & Siegel RM (2014). Optical imaging of visually guided reaching in macaque posterior parietal cortex. *Brain Struct Funct* **219**, 495–509.

Heider B, Jandó G & Siegel RM (2005). Functional architecture of retinotopy in visual association cortex of behaving monkey. *Cereb Cortex* **15**, 460–478.

Heider B, Karnik A, Ramalingam N & Siegel RM (2010*a*). Neural representation during visually guided reaching in macaque posterior parietal cortex. *J Neurophysiol* **104**, 3494–3509.

Heider B, Nathanson JL, Isacoff EY, Callaway EM & Siegel RM (2010*b*). Two-photon imaging of calcium in virally transfected striate cortical neurons of behaving monkey. *PLoS One* **5**, e13829.

Johnson PB & Ferraina S (1996). Cortical networks for visual reaching: intrinsic frontal lobe connectivity. *Eur J Neurosci* **8**, 1358–1362.

Johnson PB, Ferraina S, Bianchi L & Caminiti R (1996). Cortical networks for visual reaching: physiological and anatomical organization of frontal and parietal lobe arm regions. *Cereb Cortex* **6**, 102–119.

Kalaska JF & Green A (2007). Is the movement representation in the motor cortex a moving target? *Neuron* **54**, 500–502.

Kurata K & Hoshi E (1999). Reacquisition deficits in prism adaptation after muscimol microinjection into the ventral premotor cortex of monkeys. *J Neurophysiol* **81**, 1927–1938.

Kurata K & Hoshi E (2002). Movement-related neuronal activity reflecting the transformation of coordinates in the ventral premotor cortex of monkeys. *J Neurophysiol* **88**, 3118–3132.

Lee J-H & van Donkelaar P (2006). The human dorsal premotor cortex generates on-line error corrections during sensorimotor adaptation. *J Neurosci* **26**, 3330–3334.

Lewis JW & Van Essen DC (2000). Corticocortical connections of visual, sensorimotor, and multimodal processing areas in the parietal lobe of the macaque monkey. *J Comp Neurol* **428**, 112–137.

Li C-SR, Padoa-Schioppa C & Bizzi E (2001). Neuronal correlates of motor performance and motor learning in the primary motor cortex of monkeys adapting to an external force field. *Neuron* **30**, 593–607.

Li C-Y, Tanaka M & Creutzfeldt OD (1989). Attention and eye movement related activation of neurons in the dorsal prelunate gyrus (area DP). *Brain Res* **496**, 307–313.

Luauté J, Schwartz S, Rossetti Y, Spiridon M, Rode G, Boisson D & Vuilleumier P (2009). Dynamic changes in brain activity during prism adaptation. *J Neurosci* **29**, 169–178.

MacKay WA (1992). Properties of reach-related neuronal activity in cortical area 7A. *J Neurophysiol* **67**, 1335–1345.

Merchant H, Battaglia-Mayer A & Georgopoulos AP (2001). Effects of optic flow in motor cortex and area 7a. *J Neurophysiol* **86**, 1937–1954.

Messier J & Kalaska JF (1999). Comparison of variability of initial kinematics and endpoints of reaching movements. *Exp Brain Res* **125**, 139–152.

Mountcastle VB, Lynch JC, Georgopoulos A, Sakata H & Acuna C (1975). Posterior parietal association cortex of the monkey: command functions for operations within extrapersonal space. *J Neurophysiol* **38**, 871–908.

Mountcastle VB, Andersen RA & Motter BC (1981). The influence of attentive fixation upon the excitability of the light-sensitive neurons of the posterior parietal cortex. *J Neurosci* **1**, 1218–1225.

Newport R & Jackson SR (2006). Posterior parietal cortex and the dissociable components of prism adaptation. *Neuropsychologia* **44**, 2757–2765.

Norris SA, Greger BE, Martin TA & Thach W (2001). Prism adaptation of reaching is dependent on the type of visual feedback of hand and target position. *Brain Res* **905**, 207–219.

Padoa-Schioppa C, Li C-SR & Bizzi E (2004). Neuronal activity in the supplementary motor area of monkeys adapting to a new dynamic environment. *J Neurophysiol* **91**, 449–473.
Petermann T, Thiagarajan TC, Lebedev MA, Nicolelis MAL, Chialvo DR & Plenz D (2009). Spontaneous cortical activity in awake monkeys composed of neuronal avalanches. *Proc Natl Acad Sci U S A* **106**, 15921–15926.
Pouget A & Sejnowski TJ (1997). Spatial transformations in the parietal cortex using basis functions. *J Cogn Neurosci* **9**, 222–237.
Pouget A, Ducom J-C, Torri J & Bavelier D (2002). Multisensory spatial representations in eye-centered coordinates for reaching. *Cognition* **83**, B1–B11.
Quian Quiroga R, Snyder LH, Batista AP, Cui H & Andersen RA (2006). Movement intention is better predicted than attention in the posterior parietal cortex. *J Neurosci* **26**, 3615–3620.
Quiroga RQ, Nadasdy Z & Ben-Shaul Y (2004). Unsupervised spike detection and sorting with wavelets and superparamagnetic clustering. *Neural Comput* **16**, 1661–1687.
Quraishi S, Heider B & Siegel RM (2007). Attentional modulation of receptive field structure in area 7a of the behaving monkey. *Cereb Cortex* **17**, 1841–1857.
Read HL & Siegel RM (1997). Modulation of responses to optic flow in area 7a by retinotopic and oculomotor cues in monkey. *Cereb Cortex* **7**, 647–661.
Redding GM & Wallace B (2000). Prism exposure aftereffects and direct effects for different movement and feedback times. *J Mot Beh* **32**, 83–99.
Rokni U, Richardson AG, Bizzi E & Seung HS (2007). Motor learning with unstable neural representations. *Neuron* **54**, 653–666.
Rossetti Y, Koga K & Mano T (1993). Prismatic displacement of vision induces transient changes in the timing of eye-hand coordination. *Percept Psychophys* **54**, 355–364.
Rozzi S, Calzavara R, Belmalih A, Borra E, Gregoriou GG, Matelli M & Luppino G (2006). Cortical connections of the inferior parietal cortical convexity of the macaque monkey. *Cereb Cortex* **16**, 1389–1417.
Scott SH & Kalaska JF (1997). Reaching movements with similar hand paths but different arm orientations. I. Activity of individual cells in motor cortex. *J Neurophysiol* **77**, 826–852.
Scott SH, Sergio LE & Kalaska JF (1997). Reaching movements with similar hand paths but different arm orientations. II. Activity of individual cells in dorsal premotor cortex and parietal area 5. *J Neurophysiol* **78**, 2413–2426.
Shtoyerman E, Arieli A, Slovin H, Vanzetta I & Grinvald A (2000). Long-term optical imaging and spectroscopy reveal mechanisms underlying the intrinsic signal and stability of cortical maps in V1 of behaving monkeys. *J Neurosci* **20**, 8111–8121.
Siegel RM & Read HL (1997). Analysis of optic flow in the monkey parietal area 7a. *Cereb Cortex* **7**, 327–346.
Siegel RM, Raffi M, Phinney RE, Turner JA & Jandó G (2003). Functional architecture of eye position gain fields in visual association cortex of behaving monkey. *J Neurophysiol* **90**, 1279–1294.
Snyder LH, Dickinson AR & Calton JL (2006). Preparatory delay activity in the monkey parietal reach region predicts reach reaction times. *J Neurosci* **26**, 10091–10099.
Steinmetz MA, Connor CE, Constantinidis C & McLaughlin JR (1994). Covert attention suppresses neuronal responses in area 7a of the posterior parietal cortex. *J Neurophysiol* **72**, 1020–1023.
Stepniewska I, Collins CE & Kaas JH (2005). Reappraisal of DL/V4 boundaries based on connectivity patterns of dorsolateral visual cortex in macaques. *Cereb Cortex* **15**, 809–822.
Sugita Y (1996). Global plasticity in adult visual cortex following reversal of visual input. *Nature* **380**, 523–526.
Tanaka M, Weber H & Creutzfeldt OD (1986). Visual properties and spatial distribution of neurones in the visual association area on the prelunate gyrus of the awake monkey. *Exp Brain Res* **65**, 11–37.
Vercher JL, Magenes G, Prablanc C & Gauthier GM (1994). Eye-head-hand coordination in pointing at visual targets: spatial and temporal analysis. *Exp Brain Res* **99**, 507–523.
Waldron K & Schmiedeler J (2008). Kinematics. In *Springer Handbook of Robotics*, ed. Siciliano B & Khatib O, pp. 9–33. Springer, Berlin, Heidelberg.
Wang J & Sainburg RL (2005). Adaptation to visuomotor rotations remaps movement vectors, not final positions. *J Neurosci* **25**, 4024–4030.
Westendorff S, Klaes C & Gail A (2010). The cortical timeline for deciding on reach motor goals. *J Neurosci* **30**, 5426–5436.
Zar JH (1984). *Biostatistical Analysis*. Prentice-Hall, Englewood Cliffs, NJ.

Additional information

Competing interests

The authors have declared that no competing interests exist.

Author contributions

This study was conducted in the laboratory of R.M.S. at Rutgers University, Newark. R.M.S., A.K. and B.H. designed the experiments. A.K. and B.H. performed data collection. A.K., R.M.S., B.H. and F.M.S. analysed the data. A.K., B.H. and R.M.S. drafted the manuscript. F.M.S. developed the Euler angle analysis and provided critical revisions.

All authors have read and approved the final submission.

Funding

This work was supported by National Institute of Health Grants EY09223 and 1S10RR-1287, Whitehall Foundation, Charles and Johanna Busch Faculty Research Grant, Mind Science Foundation and Army W911NF-09-1-0116.

Acknowledgements

We thank H. Poizner and M. Raffi for contributions and J.A. Siegel, R. Meltzer, and A. Butensky for technical assistance.